J Mater Sci (2011) 46:4435–4457
DOI 10.1007/s10853-011-5499-3

REVIEW

The renaissance of unsupported nanostructured catalysts for low-temperature fuel cells: from the size to the shape of metal nanostructures

Ermete Antolini · Joelma Perez

Received: 30 November 2010 / Accepted: 22 March 2011 / Published online: 2 April 2011

Abstract A resurgence of interest in unsupported catalysts, commonly nanostructured Pt or Pt-based catalysts, for use in low-temperature fuel cells has occurred in recent years: indeed, the use of unsupported nanostructured catalysts may provide improved long-term stability during fuel cell operation compared to the carbon-supported catalysts because the carbon corrosion issue is eliminated. Catalyst utilization can be increased by developing novel nanostructures with high surface area and/or high catalytic activity. Indeed, in recent years, the strategy to increase the catalyst utilization has gone from decreasing the nanoparticle size to tailoring new nanostructures. This work presents an overview of recent studies on novel metal nanostructures for their possible use in low-temperature fuel cells, highlighting that these materials can better perform than the commonly utilized carbon-supported catalysts at similar catalyst loadings, having at the same time a higher stability.

Introduction

Fuel cells convert fuels into electricity directly without the need for combustion. Low-temperature fuel cells could be used to provide power for vehicles, portable devices and small stationary power in a way that is less damaging to the environment than current powering methods. Conventional low-temperature fuel cells such as phosphoric acid fuel cells (PAFCs) and polymer electrolyte fuel cells (PEMFCs) are on the verge of entering the market. However, making fuel cells as common and widely available as the conventional battery or internal combustion engine is proving difficult because there are several significant challenges that still need to be overcome, in particular the high cost of the components and the durability of the fuel cell. Unsupported platinum was the first practical working electrocatalyst in low-temperature fuel cells. Pt black electrodes were initially developed in the early 1960s and later became the primary electrocatalyst choice for the electrode. Pt black is metallic platinum with an average agglomerate size of approximately 1 μm and an electrochemical surface area of about 15 $m^2\ g^{-1}$. The fundamental particle size is in the order of 5–50 nm. A typical Pt black electrode had high Pt loadings ($\sim$4 mg cm^{-2}/side) and also contained a hydrophobic binder, typically polytetrafluoroethylene (PTFE) [1].

Platinum-supported catalysts (Pt particle size = 2–4 nm) for membrane-based fuel cells emerged in the late 1980s and early 1990s with the promise that they would lead to low catalyst loadings (low cost) while at the same time meeting all the performance and durability metrics for both stationary and transportation applications (40,000 and 5000 h, respectively). These catalysts have since attracted most of the attention from developers [2, 3]. Using carbon-supported Pt or Pt-alloys, high performances have been attained in H_2/O_2 fuel cells with very low loadings of catalyst (0.1–0.2 mg cm^{-2}) [4, 5].

In contrast to H_2/O_2 fuel cells, direct methanol fuel cell (DMFC) anodes typically have Pt alloy loadings of several mg cm^{-2}. A comparative study of the use of supported and unsupported catalysts for DMFCs by Liu et al. [6] showed that the performance of 0.46 mg cm^{-2} PtRu/C anode is

E. Antolini (✉)
Scuola di Scienza dei Materiali, Via 25 aprile 22, 16016 Cogoleto, Genoa, Italy
e-mail: ermantol@libero.it

E. Antolini · J. Perez
Instituto de Química de São Carlos, USP, C. P. 780, São Carlos, SP 13560-970, Brazil

comparable to the performance of anodes with 2 mg cm^{-2} of unsupported PtRu nanoparticles. The very high specific surface area of the supported PtRu catalyst is the reason for the higher catalytic activity relative to the unsupported catalysts.

It is known, however, that Pt-nanoparticle coarsening and corrosion of carbon support are the major causes for specific surface area loss of Pt/C catalysts [7–9]. Carbon corrosion and subsequent platinum sintering are primarily responsible for performance degradation when fuel cell stack operation is interrupted; the degradation rate increases with higher operating voltages. Thus, ongoing research involves finding catalyst support materials with better corrosion resistance [10] and strengthening metal–catalyst support interactions.

A resurgence of interest in unsupported catalysts has occurred in recent years: indeed, the use of unsupported nanostructured catalysts may provide improved long-term stability compared to the carbon-supported catalysts during fuel cell operation because the carbon corrosion issue is eliminated. Moreover, in DMFCs, unsupported catalysts allow very thin catalytic layers to be used, even in presence of significant loadings (e.g. 2 mg_{Pt} cm^{-2}). This leads to a reduction of ohmic drop [11] and facilitates migration of the reacting species through the catalyst layer [12].

In general, the mass activity (MA, activity $mass^{-1}$) of a catalyst is defined as the current normalized by the noble metal loading or catalyst loading as measured at a specific potential, and can be expressed as:

$$\mathrm{MA} = \mathrm{SA} * \mathrm{SSA} \quad (1)$$

where SA is the specific activity (activity $area^{-1}$), defined as the current normalized by the chemical (CSA) or electrochemically active (ECSA) surface area and SSA is the specific, chemical or electrochemically active, surface area (area $mass^{-1}$). The use of ECSA is more appropriate than CSA for the definition of the SSA area of a catalyst. Indeed, a not negligible part of noble metal atoms presents on the catalyst surface are not electrochemically active, being not accessible to reactants, due to the presence of an excess of oxides or being localized inside small pores. To increase catalyst utilization, novel Pt nanostructures with improved SSA and/or SA have been developed. In the recent years, the strategy to increase the catalyst utilization has gone from decreasing the nanoparticle size to tailor new nanostructures with high surface area and/or high specific activity. The use of nanostructured Pt and Pt-based catalysts in fuel cells has only been discussed briefly in recent reviews of such catalysts [13–16]. In this work, an overview of recent studies on novel metal nanostructures for their possible use in low-temperature fuel cells is presented, highlighting that these materials can perform better than the commonly utilized carbon-supported catalysts at similar catalyst loadings, having at the same time a higher stability.

Improving mass activity: from the size to the shape of metal nanostructures

As previously reported the MA can be increased (and thus the platinum loading can be lowered) by increasing the specific surface area of the catalysts, i.e. by decreasing the particle size. It is generally accepted that the oxygen reduction reaction (ORR) SA changes with particle diameter activity. This in turn means that MA is not simply inversely proportional to particles size. As a first approximation, $\mathrm{SSA} = k\ 1/d$ and $\mathrm{SA} = k'\ \ln\ d$, where d is the particle size, k is the SSA for $d = 1$ nm and k' is the SA for $d = e = 2.7$ nm. By setting the derivative of MA versus d equal to 0 [$d(\mathrm{MA})/d(d) = 0$], the value of d for maximum MA is the exponential $e = 2.7$. According to literature, the experimental optimum crystallite size for the ORR on polycrystalline Pt nanoparticles in acid electrolytes is about 3 nm [17–19]. It was suggested that the change in the fraction of surface atoms on the {100} and {111} crystal faces of Pt particles, going from smaller spherical to larger cubo-octahedral structures, can be correlated to SA and MA of highly dispersed Pt electrocatalysts. The maximum in MA was attributed to the maximum in the surface fraction of Pt atoms on the {100} crystal face, resulting from the change in surface coordination number with a change in the particle size [17]. On the other hand, according to Gamez et al. [20], the particle size effect results from stronger adsorption of oxygenated intermediate species on smaller particles, which hinders the ORR. All these experiments referenced above [17–20] were measured in H_2SO_4. It has been suggested that, as sulfate anions can diffuse from the aqueous electrolyte to the active layer, the size effect could also partly result from adsorption of these anions on Pt [21]. A Pt particle size effect on the ORR, however, was also observed in non-adsorbing $HClO_4$ [22–24]. The origin of particle size effects on the ORR in those studies was attributed to stronger interaction of oxygenated species with smaller Pt particles, due to the dependence of Pt electronic state [22, 23] or of the potential of point of zero charge [24] on particle size. Considering the excellent agreement observed between the ORR activities measured in $HClO_4$ and by PEMFC testing, Gasteiger et al. [25] confirmed that the same particle size effects were observed in PEMFCs. The particle size can affect not only the ORR, but also the methanol oxidation reaction (MOR) [26–28]. The

dependence of the MOR activity on the particle size was attributed to the stronger binding of OH and CO (formed by methanol decomposition) on smaller particles.

In addition to the size, the shape or morphology of a Pt nanoparticle provides a powerful tool for tuning its electrocatalytic properties. Thus, as well as studies on the dependence of platinum activity and durability on particle size, the shape-dependent properties of nanostructured platinum have also been explored, showing that the catalytic activity can be related to the shape of platinum nanostructures [13–16, 29]. The use of unsupported, novel nanostructures with high SSA and/or SA is emerging as an alternative to conventional methods (reducing particle size by dispersing a catalyst on a carbon support). Metal nanostructures with a variety of shapes and morphologies have been explored, such as nanotubes, nanowires, nanodendrites, nanoflowers, meso/nanoporous structures, nanocubes, nanomultioctahedrons, and nanotetraexahedrons. It has been found that the catalytic activity of these metal nanostructures is higher than that of spherical metal nanoparticles. In the next sections, some novel metal nanostructures are presented and their catalytic activity and stability is compared with that of conventional unsupported and supported nanoparticles. Although these metal nanostructures can possess both high specific surface area and high specific activity, they have been separate in two classes, according to the scheme reported in Fig. 1, showing the relation between the particle shape and the mass activity, based on their main characteristics.

Thermodynamic and kinetic aspects affecting the shape of nanostructures

The control of the size and shape of platinum materials at the nanoscale can contribute to lowering the amount of Pt utilized, thereby achieving the desired cost reductions [13]. The shapes of platinum and platinum-based nanoparticles can be controlled by both thermodynamic and kinetic factors, which are determined by both the intrinsic structural properties of platinum and the reaction conditions, for example solvent, capping agent, and reducing agent [14]. Metal nanoparticles form facets to minimize surface energy and total excess free energy. Platinum, which has the face-centered cubic (fcc) symmetry, is usually bound by three low-index planes, namely {100}, {110}, and {111} surfaces. The surface energies (γ) of the low-index crystallographic planes are in the order of $\gamma\{111\} < \gamma\{100\} < \gamma\{110\}$. In general, the non-spherical particle shape originates from a combination of the final stability of different facets due to the different growth rate of {111} and {100} faces. For example, a tetrahedron is bounded by {111} facets and a cube is covered by {100} facets, whereas a cuboctahedron is enclosed by a mix of {100} and {111} facets. While the "simple" shapes including tetrahedron, cube, octahedron, and their truncated forms are morphologies that can be predicted for a fcc crystal, the introduction of defects can effectively break down the crystal symmetry resulting in the formation of shapes with reduced symmetry such as nanorods, plates, planar tripods, and multipods. Figure 2 shows some possible

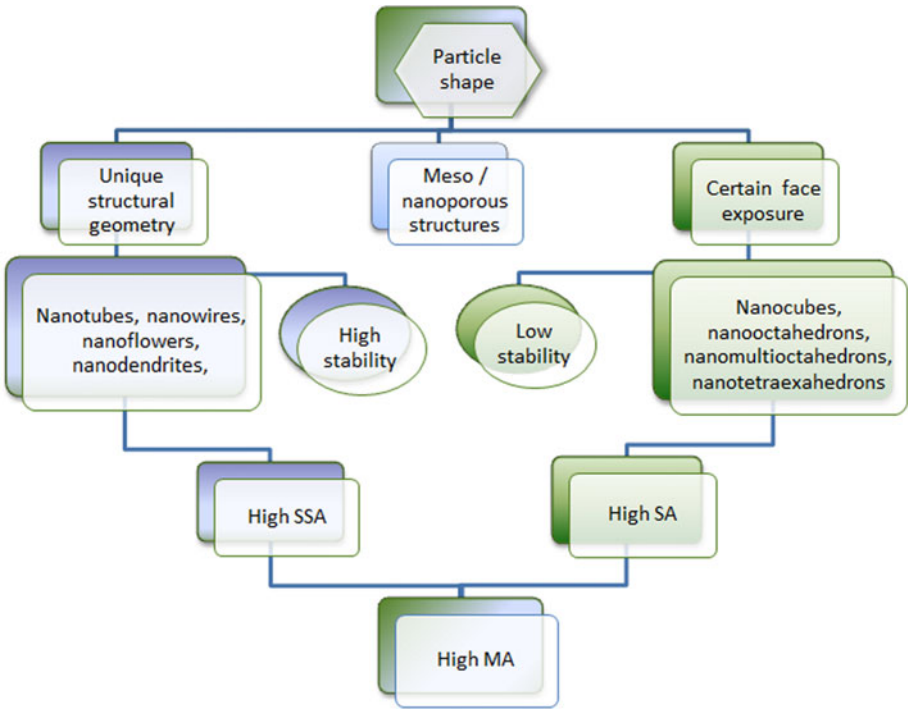

Fig. 1 Scheme of the relation between the particle shape and the mass activity of metal nanostructures

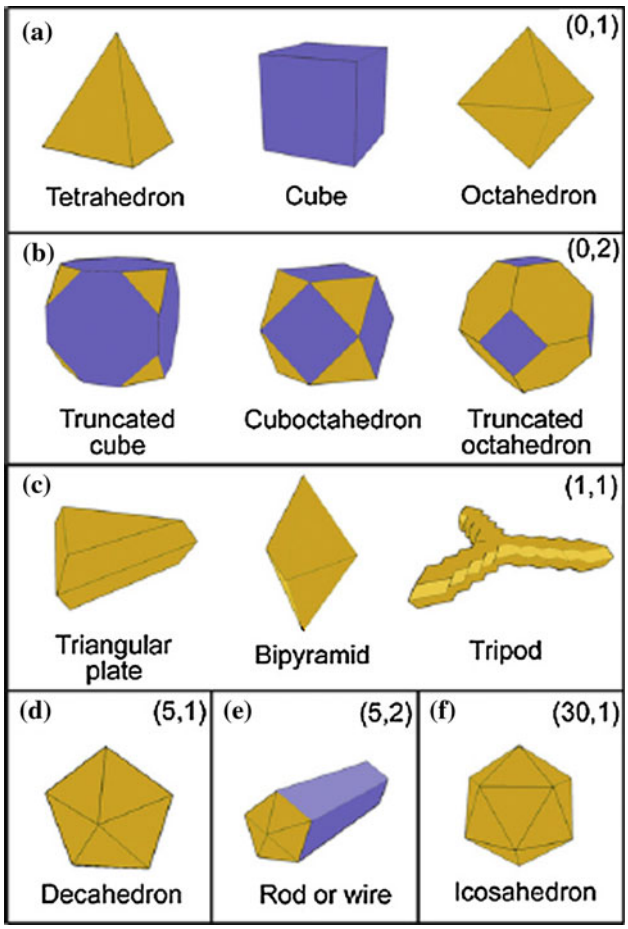

Fig. 2 Selective possible shapes of platinum nanoparticles (**a** and **b**) without defects and bounded by **a** one group and **b** two groups of facets; and (**c**–**f**) with different numbers of defects. The notation (*m*, *n*) represents the number of defects *m*, and different facets *n*, in crystals. Reproduced from [14], copyright 2009, with permission from Elsevier

shapes of platinum nanostructures with {111} and {100} planes exposed. The blue and yellow colors represent the {100} and {111} facets, respectively. A shape factor notation (*m, n*) is used to describe nanocrystals that have different numbers of defects *m*, and facets *n*. The energetically favoured shape of an fcc single Pt crystal would be a truncated octahedron with the optimal truncation fulfilling the condition of $\gamma\{100\}/\gamma\{111\} = l\{100\}/l\{111\}$, where l represents the distance from the facet to the center of the particle and this parameter reflects the ratio of growth rates along {100} and {111} directions [30]. The ratio of these two growth rates can be defined as R, which changes from 0.58 for a cube to 0.87 for a cuboctahedron and eventually to 1.73 for an octahedron. The surface energies and thus growth rates can be modified by using various capping agents in a shape-controlled synthesis. Both the selectivity of a capping agent for a specific facet and its concentration play important roles in the formation of well-defined polyhedrons. The shapes of platinum nanoparticles can be controlled by changes in the ratio of the concentration of the capping polymer material to the concentration of the platinum cations used in the reductive synthesis of colloidal particles. Tetrahedral, cubic, irregular-prismatic, icosahedral, and cubo-octahedral particle shapes have been observed, whose distribution was dependent on the concentration ratio of the capping polymer material to the platinum cations [31]. The difference between the rate of the catalytic reduction process of Pt^{2+} on the {111} and {100} faces, the competition between the Pt^{2+} reduction and the capping process on the different nanoparticle surfaces, and the concentration-dependent buffer action of the polymer itself all control the final distribution of the different shapes observed.

Multiple factors can affect size and shape of platinum nanoparticles produced in a solution through the nucleation and growth process [14]. At initial stages, the zero-valence metal atoms form through either reduction of ions or bond breaking of compounds. These metal atoms collide to produce small clusters that are thermodynamically unstable and can dissolve before they reach a critical radius or overcome a critical free energy barrier and become thermodynamically stable nuclei. These nuclei grow into nanoparticles at the consumption of free atoms in solution or unstable small clusters. The seed structures in the nucleation step can be influenced by controlling the reaction kinetics. In this way, it is possible to obtain Pt nanocrystals of different morphologies through the control of reaction kinetics by varying reduction conditions [13]. When the reduction is relatively fast, the nanocrystallite seeds tend to grow and form the thermodynamically favoured shape (i.e., truncated octahedron) in an effort to minimize the surface energy. When the reduction is slowed down, the shape of a Pt nanocrystal becomes more sensitive to the capping agent. The promotion or inhibition of selective growing surfaces or the relative stability of these surfaces should be the key to achieve a desired shape. Through the shape-controlled synthesis, it is possible to address the shape of a nanocrystal to only expose a specific set of facets.

Synthesis methods of unsupported Pt and Pt-based catalysts

Conventional unsupported spherical/cubo-octahedral nanoparticle catalysts

Various methods are utilized for preparing conventional unsupported spherical/cubo-octahedral nanoparticle catalysts. A commonly used synthesis method is the reduction of Pt precursors (and M precursors in the case of binary PtM catalysts) in aqueous solution at low temperature

(<100 °C) or at intermediate temperature (250–500 °C) with $NaBH_4$, hydrazine, or hydrogen [32, 33].

Colloid methods are widely used to prepare Pt and Pt-based catalysts. The polyol process is a technique in which a polyol such as ethylene glycol is used as both solvent and reducing agent. A unique property of the polyol process is that it does not require any type of polymer stabilizer. In the polyol process using ethylene glycol, metal ions are reduced to form a metal colloid by receiving the electrons from the oxidation of ethylene glycol to glycolic acid. Glycolic acid is present in its deprotonated form as glycolate anion in alkaline solution. It is believed that the glycolate anion acts as a stabilizer by adsorbing the metal colloids. Stable platinum metal nanoclusters with small particle size in organic media have been prepared by heating corresponding metal hydroxide colloids in ethylene glycol containing NaOH [34]. Bonnemann et al. [35] developed a colloidal method to prepare unsupported metals and alloys. Metal salts of Groups 6–12 were reduced using alkali hydrotriorganoborates in hydrocarbons between −20 and 80 °C to give boron free powder metals. The use of tetraalkylammonium hydrotriorganoborates as reducing agents leads to colloidal transition metals in organic phases. These colloids may also be obtained using conventional reducing agents after first reacting the metal salts with the stabilizing tetraalkylammonium halide. Preparation of nanoparticles using a microemulsion provides a convenient control of size and composition. Oil-continuous microemulsions in which well-defined closed aggregates occur are expected to form an ideal environment for the formation of very small colloidal particles. The reducible ions can be dissolved to high concentrations in the thermodynamically stable aqueous "nuclei" of the microemulsion, while the "nuclei" still are separated. from one another by a non-aqueous environment. Unsupported Pt–Co catalysts were prepared by Zhang et al. [36] using a water-in-oil reverse microemulsion system, with hydrazine as reducing agent. The reduction reaction occurs in a confined reaction zone within the microemulsions. The ultimate nanoparticles should follow the metal composition in the precursor solution, without losing control of particle size.

Organometallic compounds as precursors are also used to prepare unsupported nanosized Pt and Pt-based catalysts. By thermal decomposition or reducing of organometallic precursors, small nanoparticles of metal or alloy with narrow size distribution can be obtained [37, 38].

New unsupported nanostructured catalysts

A number of shapes have been achieved for Pt nanostructures using different synthesis methods. In general, shape-controlled Pt nanostructures are synthesized by the same synthesis methods used to prepare conventional Pt-based unsupported nanoparticles but in the presence of organic-capping agents and/or inorganic ions, by electrochemical synthesis (exceptional shapes), by template-assisted synthesis, or by electrochemical dealloying.

Synthesis in the presence of organic-capping agents

organic-capping agents are widely used in shape control of colloidal platinum nanostructures. Long carbon chains of organic-capping agents are hydrophobic and have the stereo hindrance effect to prevent direct contacts among relatively high energy surfaces of platinum, stabilizing in this way Pt nanoparticles. The decrease in total excess free energy, due to the adsorption of capping agents, effectively prevents Pt nanoparticles from further growth and Ostwald ripening. When capping agents adsorb selectively onto given platinum surfaces, the morphology of the nanostructures can be controlled. The preferred adsorption onto one set of surfaces results in different growth rates along various given crystallographic directions. The solute atoms would more likely attach to those less protected platinum surfaces, leading to an anisotropic growth. One key criterion in selecting capping agents for shape control is the kind of interaction between the capping agents and the various platinum facets, affecting the adsorption and desorption processes. Capping agents commonly used in the synthesis of nanostructurred Pt are poly(vinyl pyrrolidone) (PVP), sodium polyacrylate, tetradecyltrimethylammonium bromide (TTAB), oleic acid, and oleylamine. By using PVP, eventually in the presence of inorganic ions, Pt nanowires, Pt nanocubes, and Pt nanomultioctahedrons have been obtained, as well as Pt nanoflowers and Pt nanocubes have been synthesized with oleylamine as the capping agent. As previously reported, the concentration of the capping agent play an important role in the formation of well-defined polyhedrons. Indeed, the reduction of K_2PtCl_4 by H_2 gas in aqueous solutions lead to different shapes of Pt nanostructures, depending on the concentration of sodium polyacrylate [31]. Pt tetrahedrons were stabilized at high concentrations of sodium polyacrylate. At low concentrations of sodium polyacrylate, instead, formation of cubes occurred, due to the deposition of Pt atoms on the {111} facets. When the reduction rate is slowed down, the shape of a Pt nanocrystal becomes more sensitive to the capping agent. TTAB is an effective capping agent, which preferentially adsorb to {100} surfaces of platinum in aqueous solutions. Pt cuboctahedrons and cubes have been prepared in the presence of TTAB by reducing K_2PtCl_4 with H_2 generated in situ from the hydrolysis of $NaBH_4$ [39]. The amount of H_2 production, which determines the reduction rate, can be controlled by adjusting the pH. At low pH, large amount of H_2 was produced and cuboctahedrons

were formed at fast reduction rate by taking the thermodynamically favored shape. At high pH, small amount of H_2 was generated and selective growth along {111} directions of cuboctahedrons led to the formation of cubes at slow reduction rate. Replacing $NaBH_4$ with ascorbic acid, a milder reducing agent, Pt nanodendrites were obtained as the final products [39].

Synthesis in the presence of inorganic ions

Inorganic ions play increasingly important roles in the design of shape-controlled platinum nanoparticles. Similar to the role of adsorptive organic molecules, these inorganic species show preferred adsorption to specific facets of platinum. Unlike their organic counterparts though, such interactions can either promote or inhibit the further growth along given directions. Silver and iron species are the most used inorganic ions in the synthesis of nanostructured Pt. Silver adsorbs preferentially on {100} surfaces in the form of either Ag^0 or Ag_4^{2+}, enhances the crystal growth rate along {100}, and essentially determines the shape and surface structure of the Pt nanocrystals [40]. Cubic, cubo-octahedral, and octahedral shapes of Pt nanoparticles have been prepared by adding different amount of silver ions in the reaction mixtures [40]. Chen et al. [41] observed that the shape of Pt^0 nanostructures obtained by polyol synthesis can be altered by introducing trace amount of Fe(II) and Fe(III) ions, which mediate the reduction rates of Pt(IV) species on various surfaces of platinum differently. Kinetic control is achieved by coupling the reduction with an Fe^{II}/Fe^{III} redox reaction. The iron species play a key role in inducing the formation of multioctahedral structures by decreasing the concentration of Pt atoms and keeping a low concentration for the Pt seeds during the reaction [42]. This condition favors the overgrowth of Pt seeds along their corners and thus the formation of multiarmed nanocrystals. The size of the multioctahedral Pt nanocrystals can be controlled by varying the concentration of $FeCl_3$ and/or the reaction temperature.

Electrochemical synthesis of exceptional shapes

Many unconventional polyhedrons, that is, tetrahexahedrons bound by {$hk0$}, trapezohedrons by {hkk}, trisoctahedrons by {hhl}, and hexoctahedron by {hkl} with $h > k > l$, are hard to produce using an ordinary chemical method as their surface energies are too high. Nevertheless, Pt nanocrystals in the tetrahexahedral shape have recently been obtained by electrochemically treating spherical particles of Pt deposited on glassy carbon with a square-wave potential in the presence of ascorbic acid and sulfuric acid [43]. For a tetrahexahedron, the nanocrystal exhibits O_h symmetry and is enclosed by 24 high-index facets, which can be viewed as a cube with each face capped by a square-based pyramid. In the electrochemical treatment, the square-wave potential was believed to mediate the adsorption behavior of oxygen on various facets of Pt particles, leading to the formation of such an exceptional shape. The oxygen atoms could preferentially adsorb onto the high-index facets and preserve these surfaces. In contrast, it was difficult for the oxygen atoms to absorb onto the low-index facets. Instead, they simply displaced the Pt atoms on these surfaces, resulting in disappearance of these facets.

Template-assisted synthesis

In recent years, many research activity focused on the synthesis of new ordered porous materials by utilization of porous matrices as templates [44]. Unlike the previously described synthesis methods, which chemically or electrochemically promote or inhibit the growth of the nanostructure along given directions, affecting the thermodynamic or kinetic parameters of Pt growth, templates offer confined spaces and/or functionalized structures for the growth of platinum. Templates can be classified into two main categories: hard and soft templates. In general, hard templates (carbon nanotubes, mesoporous silica, and anodic aluminum oxide) have been successfully used to prepare platinum and platinum alloy nanotubes and nanowires, whereas soft templates (liquid crystal-templating materials, micelle, reverse micelle, microemulsion, and liposome) have been utilized to synthesize mesoporous platinum and platinum nanodendrites. The obtained Pt nanostructures are polycrystalline and have controllable pore sizes, high surface areas, and large pore volumes.

Electrochemical dealloying

Dealloying is a selective corrosion process where the less-noble constituent of an alloy is removed, usually by dissolving it in a corrosive environment with an applied potential (electrochemical dealloying) or without (chemical dealloying). By controlling the temperature of dealloying, the amount of the alloying metal, the potential applied, the time of dealloying, and the corrosive used, the size of the pores and ligaments within the porous material can be fine-tuned. Electrochemical dealloying leads to a 3-dimensional nanoporous structure formed of nanocrystalline foam ligaments.

Metal nanostructures with high specific surface area

To date, efforts are addressed to the development of techniques to produce catalysts with a high surface area to

achieve high catalytic performance and utilization efficiency. Metal nanostructure with high specific surface area can be in form of hollow microsphere (mesoporous Pt [45] and Pt nanotubes [46]), foamlike nanospheres, and nanosheets (Pt dendritic sheets [47]) or linear structure arrays (Pt and Pd nanowires [48, 49]). Hollow structures with at least one nanoscaled dimension could combine both advantages of the dimensions and high space utilizations, and offer a uniquely high surface area compared to their solid counterparts. Commonly, these materials are polycrystalline, and, as a consequence are not selective.

Nanostructures with unique structural geometry

One-dimensional structures: nanotubes and nanowires

Nanotubes (NTs) and nanowires (NWs) have attracted significant interest as a result of their peculiar properties, imposed by the anisotropy of their one-dimensional (1D) geometry. Conventional platinum nanotubes (PtNTs) are made of seamless cylinders of platinum networks. The tubular structure of platinum nanotubes makes them unique among different forms of platinum. Because of their unique combination of dimensions at multiple length scales, nanotubes can provide high platinum surface area as a result of having nanometer-sized wall thicknesses. At the same time, these materials have the potential to eliminate or significantly reduce degradation pathways observed in Pt/C by support corrosion. Moreover, the micrometer-sized length of the PtNTs makes them less vulnerable to dissolution. Platinum nanowires (PtNWs) and palladium nanowires (PdNWs) are a class of one-dimensional nanomaterials with a high aspect ratio and solid core. The co-existence of both the hollow (nanotubes) and solid (nanowires) filled structures was observed in Pt samples generated from membrane templates [50]. In effect, nanotubes and nanowires represent different stages of Pt nanostructure growth. Either nanotubes or nanowires of PtRu alloys can be obtained by electro-codeposition through a porous membrane, depending on the metal precursor concentration in the electrolyte [51]. Synthesis of PtNTs is commonly realized through two methods, either galvanic displacement or using selected templates [15]. A relatively high yield of nanotubes is obtained with the galvanic displacement approach, however, the dimensions and wall thickness of the resultant hollow structures cannot be independently varied. The template-assisted approach, on the other hand, seems to be more beneficial in forming nanotubes with controllable wall thickness. For the synthesis of PtNWs with well-controlled aspect ratio, several routes have been proposed such as the template-assisted method and the colloidal route using surfactants/capping molecules. In former case, both soft (micelle) and hard templates (carbon nanotubes, mesoporous silica, and porous alumina membrane) have been successfully used for preparing PtNWs. This route provides several distinct advantages over the latter method, offering a convenient way for producing structurally uniform and often periodically aligned materials in template matrices. In general, these structures are polycrystalline. The high catalytic activity of these 1D nanostructured materials is due not only to their high surface area, but also to their structural geometry. Among the different nanostructured Pt materials, PtNts and PtNWs presented the highest stability upon potential cycling.

In some works, the chance to substitute carbon-supported Pt with PtNTs as catalysts in low-temperature fuel cells has been investigated. The catalytic activity and stability of PtNTs has been compared to that of conventional unsupported and carbon-supported Pt. Chen et al. [46] found that both the mass activity and the specific activity for oxygen reduction of PtNTs, synthesized by galvanic replacement using silver nanowires as the substrate, are higher than those of commercial platinum-black and Pt/C catalysts. Durability tests showed a significant decrease of platinum ECSA for platinum-black and Pt/C, and only a small decrease for PtNTs; PtNT ECSA only decreased about 20% after 1,000 cycles, while platinum-black and Pt/C catalysts had an ECSA loss of about 51 and 90%, respectively. Following repetitive potential cycling (RPC), the particle size of the Pt/C catalyst increased from 2–5 to 10–20 nm, confirming that the major cause for the ECSA loss of Pt/C is platinum nanoparticle ripening and to aggregation owing to carbon corrosion, and the particle size of platinum-black increased from 5–10 to 10–25 nm, as a result of surface-energy minimization and Ostwald ripening. Conversely, there was no noticeable morphological change for the PtNTs. Using the same synthesis method, Bi and Lu [52] obtained PtNTs with uniform density of nanoshells and highly crystalline walls throughout the tubes. PtNTs ECSA was higher than that of Pt/C, and the MOR activity of PtNTs was nearly four times higher than that of Pt/C. Ordered polycrystalline Pt [53] and Pt–Cu [54] nanotube arrays were fabricated by one-step electrodeposition utilizing nanochannel alumina (NCA) templates. Scanning electron microscopy (SEM) images of the PtNT arrays are shown in Fig. 3. Figure 3a shows the surface of the free-standing PtNTs with length of about 750 nm after completely dissolving the NCA template. The inset in Fig. 3a shows the SEM image of the NCA template filled with PtNT arrays: it can be seen that the PtNTs replicate the pore sizes and shapes. Figure 3b shows a high magnification SEM image of the oblique view of the PtNTs. PtNTs have rough surfaces, and dispersed nanosized particles can be observed on both the inner and outer surfaces, revealing that the PtNTs are formed by the inhomogeneous accumulation of nanoparticles. The oxidation peak currents for ethanol

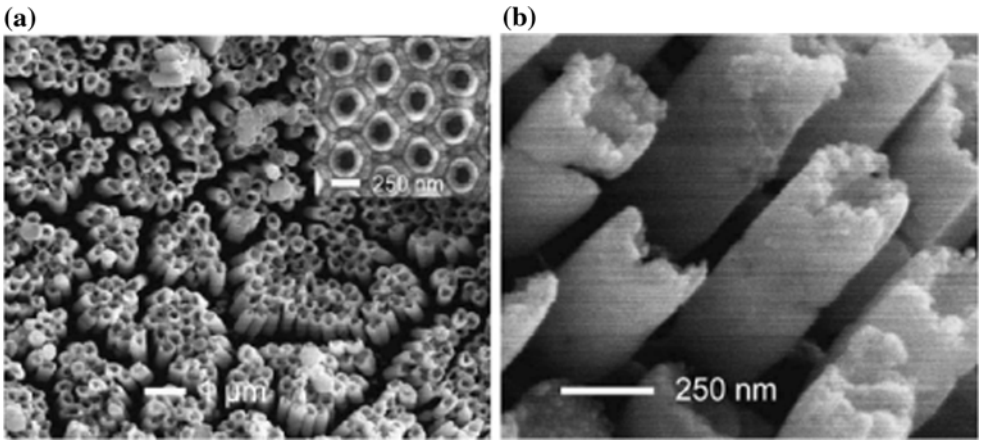

Fig. 3 SEM images of Pt nanotube arrays: **a** low magnification; **b** high magnification. Reproduced from [53], copyright 2009, with permission from Elsevier

electro-oxidation on the PtNT array electrode were about 1.7 times those on the commercial PtRu/C electrode, making it a promising catalyst for direct ethanol fuel cells (DEFCs). Recently, Górzny et al. [55] used a novel method for the synthesis of platinum-tobacco mosaic virus (Pt-TMV) nanotubes. A platinum salt was reduced to its metallic form on the external surface of a rod-shaped TMV by methanol. The ECSA of the Pt-TMV nanotubes was in the range 14–32 $m^2\ g^{-1}$. When used as a catalyst for methanol oxidation, these Pt nanotubes displayed a 65% increase in the mass activity compared to that of Pt nanoparticles. Stability tests showed that, while Pt-TMV nanotubes lose between 8 and 24% of their ECSA, Pt nanoparticles lose 50–65% of their ECSA after 400 cycles.

In general, the improved activity of the Pt nanotubes was ascribed to their high surface area, high Pt utilization and the exposure of certain crystal facets. Furthermore, these Pt nanotubes, like carbon nanotubes, have an anisotropic morphology and inner walls that can improve mass transport and catalyst utilization for the electrocatalytic reactions. It is important to point out, however, that all the catalytic activity and stability tests on these PtNTs have been carried out by cyclic voltammetry (CV) in acid or alkaline medium, and none of these nanostructures has been tested in a fuel cell.

Various articles have addressed the possible use of PtNWs and PdNWs as catalysts for methanol and ethanol oxidation in low-temperature fuel cells. Highly ordered PtNWs [56] and PdNWs [49] arrays were prepared by electrodeposition, using anodic aluminum oxide (AAO) as a template. PtNWs and PdNWs presented a uniform diameter, retaining the size and near cylindrical shape of the pores of the template. The Pt nanowire array electrode showed higher MOR activity than flat Pt and good stability [56]. In the same way, the Pd nanowire arrays presented high ECSA and showed excellent activity for the ethanol oxidation reaction (EOR) in alkaline media. The EOR activity of PdNW arrays was not only higher than that of Pd film, but also higher than that of commercial PtRu/C [49]. PtNWs with high MOR activity [57] and PdNWs with high EOR activity [58] were synthesized by electrodeposition of Pt precursors containing PVP, and by using hexagonal mesophases as templates, respectively. The high catalytic activity of PtNW and PdNW arrays may be attributed to the micrometer sized pores and channels in nanowire arrays. They allow liquid fuels to diffuse into and products diffuse out of the catalyst layer of the catalysts layer much easier, therefore, the utilization efficiency of catalysts gets higher. Thus, Pt and Pd nanowire arrays could have good potential applications in direct alcohol fuel cells (DAFCs). Kim et al. [59] prepared Pt nanowires by treating electrospun PVP–Pt composite fibers at high temperatures in an air atmosphere. The electrospun PVP–Pt composite fibers thermally decompose at 250 °C, which leads to the removal of 98 wt% of the PVP and the simultaneous reduction of the Pt precursor to a Pt nanowire. Furthermore, polymer fibers subjected to a pyrolization process in nitrogen followed by exposure to an air atmosphere enhance the surface area of the Pt nanowires, leading to a high MOR activity. Song et al. [48] synthesized PtNW networks with uniform wire diameters by using a network of wormlike micelles as a soft template for metal growth. Transmission electron microscopy (TEM) images revealed the presence of abundant PtNWs in a low-magnification image (Fig. 4a). At higher magnification (Fig. 4b), the nanowires are seen to interconnect to form large extended wire networks. A high-resolution TEM (HR-TEM) image (Fig. 4c) shows that the interconnected nanowires are polycrystalline as revealed by the varied orientations of the atomic lattice fringes along an individual continuous wire. The SEM image in Fig. 4d shows how the nanowire network forms a three-dimensional porous

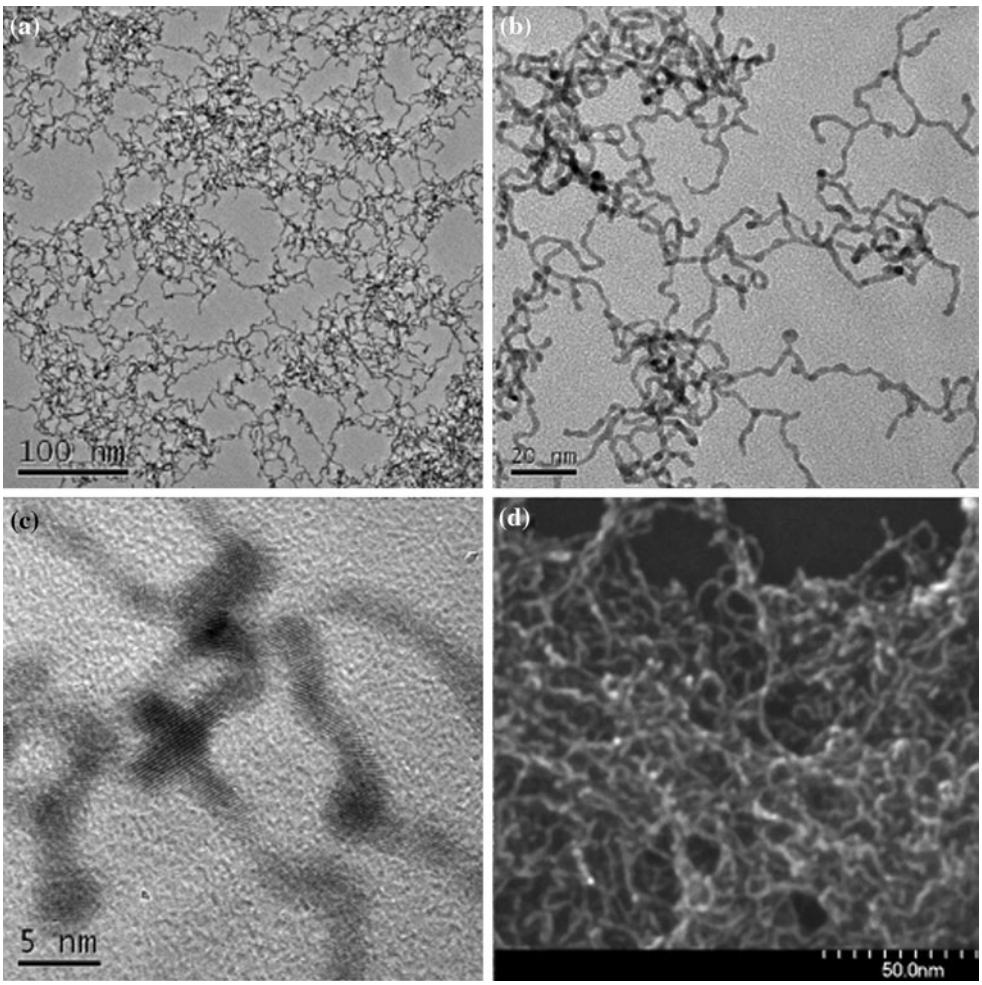

Fig. 4 TEM images (**a**, **b**), HRTEM image (**c**), and SEM image (**d**) of the platinum-nanowire network. Reaction conditions: 20 mM Pt(II) and 40 mM CTAB in 10 mL of chloroform; 30 mM $NaBH_4$ in 100 mL of water; stirring at 1,000 rpm. Reproduced from [48], copyright 2007, with permission from the American Chemical Society

mass and also verifies that the diameters of the PtNWs are uniform. The PtNW network presented a high electroactive surface area (32 m^2 g^{-1}), comparable to that of mesoporous Pt. Polycrystalline PtNWs were prepared via a template-synthesis method by electrodeposition of platinum within pores of a track-etched polycarbonate membrane [60]. The electrocatalytic activities of PtNWs, Pt/C, and Pt black were compared by varying the Pt content on the electrode from 0.2 to ca. 3 mg_{Pt} cm^{-2}. For high Pt loadings, the PtNWs showed the highest mass activities and stability for hydrogen and methanol electro-oxidation. Thus, Pt nanowires may be promising electrocatalysts for DAFCs requiring high Pt content. Preferentially oriented {100} PtNW arrays were synthesized by the use of a potentiostatic deposition through a porous AAO membrane [61]. PtNWs showed an increased resistance to ECSA loss upon RPC in acidic solution, as compared to Pt black. The RPC, however, leads to a strong perturbation of platinum surfaces and the preferential {100} orientation was no longer observed. Although the mechanisms underlying the formation of preferentially oriented {100} surface remain to be elucidated, these PtNWs seem an ideal choice of material in the case of surface structure sensitive electrocatalytic reactions which require high roughness factors (specific surface area to geometrical surface area ratios) coupled with preferential {100} platinum surfaces. Yuan et al. [62] synthesized branched Rh/Pt bimetallic ultrathin nanowires with nodes and stems by a seed displacement, epitaxial growth method. Rh/Pt nanowires presented enhanced electrocatalytic performance and selectivity toward ethanol oxidation than commercial Pt black. The selectivity to the complete oxidation of ethanol to CO_2 of Rh/Pt nanowires was at least 2.69 times higher than that measured on commercial Pt black. Koenigsmann et al. [63] employed an acid-wash protocol to obtain highly exfoliated, crystalline PtNWs with a diameter of 1.3 ± 0.4 nm. The ORR activity of these PtNWs was nearly four times greater than that of analogous, unsupported platinum

nanotubes and seven times greater than that of commercial Pt/C.

Liang et al. [64] and Du [65] tested PtNWs as electrode materials in DMFCs and PEMFCs, respectively. Liang et al. [64] proposed a new DMFC anode structure consisting of PtNWs electrochemically deposited into a partial layer of a Nafion membrane. The platinum-nanowire network formed not only provides the electron conduction paths but also functions as the catalyst for the MOR, while the remaining part of the membrane with no Pt keeps on the function as the electrolyte. The Pt-Nafion integrated electrode possessed a larger ECSA than the conventional E-TEK electrode. The DMFC with this new anode structure presented a lower rate of methanol crossover as the result of the incorporation of PtNWs into the hydrophilic pores of the membrane. DMFC tests further showed that the integrated electrode better performs than the conventional electrode.

Du developed a very simple and effective process for preparing gas diffusion electrodes (GDEs) in PEMFCs [65]. PtNWs were grown on the carbon fibers in the carbon paper by reducing H_2PtCl_6 with formic acid in the presence of PVP at room temperature, without using any template or catalyst. The PtNWs were uniformly distributed on the support surface, with a length of 100–150 nm. Impedance spectroscopy and polarization curve measurements in a PEMFC showed that the as-prepared GDE possess a lower charge transfer resistance and a higher power density than the conventional GDE. The excellent performance obtained and the simple steps made the process a promising technique for preparing GDEs in PEMFCs for commercial applications.

Bi- and three-dimensional branched structures: nanodendrites and nanoflowers

Because of their higher structural complexity and surface area compared to nanowires and nanotubes, these branched nanostructures have potential applications as catalysts and electrocatalysts.

Nanodendrites (NDs) are structures developing a typical multi-branching *tree-like* form. These structures form a natural fractal pattern. Dendritic nanostructures can be formed by metals, such as Pt and Pd, and metal oxides. Among various tactics, design and synthesis of platinum nanodendrites (PtNDs) with interconnected arms provid a promising strategy to improve the specific surface area of platinum nanomaterials. Furthermore, the presence of open dendritic nanostructures in the PtNDs structures can contribute to the high accessibility of guest species, and the rich edges and corner atoms derived from the dendritic structures of the PtNDs are highly desired for enhancing the catalytic performance [66]. Song et al. [47] reported the synthesis of novel dendritic platinum sheets by the reduction of a metal complex with ascorbic acid in the presence of liposomes. Variation of the reaction conditions, including incorporation of a tin porphyrin photocatalyst within the liposomal bilayer to initiate seed-particle growth, allows access to a diverse range of platinum nanostructures, including dendritic nanosheets of uniform diameters and convoluted foamlike structures composed of interwoven dendritic nanosheets. All of these materials are composed of flat or convoluted dendritic sheets of platinum metal that are nominally 2-nm thick with 3–4-nm wide arms and 1–2-nm arm spacings. The platinum foams are very attractive from the standpoint of electrocatalytic reactions such as in PEMFC applications. The ECSA of Pt black (ETEK) and Pt nanospheres with 140-nm and 78-nm liposomes were 15.5, 16.8, and 18.1 $m^2\ g^{-1}$, respectively. Not only they have high ECSA, but the extended open dendritic structures may provide better current conductivity than Pt black nanoparticles. These platinum foam nanospheres have the same ORR activity than commercial platinum-black. To determine whether the ripening-resistant dendritic platinum nanostructures might be durable in electrocatalytic applications, flat dendritic Pt nanosheets (Fig. 5a) and foamlike Pt nanospheres (Fig. 5b,c) composed of convoluted dendritic nanosheets were fabricated into fuel cell MEAs and the durabilities of the MEAs were evaluated [67]. The foamlike nanospheres were investigated because the interior nanosheets are locked into a rigid structure. Thus, the rapid particle-like ripening processes that may occur at the interfaces between stacked flat Pt dendritic sheets should be largely eliminated. The changes in the current densities of the MEAs during nominal 75 h fuel cell tests at 0.5 V are shown in Fig. 6a. After a brief initial increase in current density, the MEA made from the foamlike Pt nanospheres (magenta line) exhibits no current degradation over the course of the test. Conversely, the decline in current density for the Pt black MEA (black line) was 47% in 70 h. The current density for the flat Pt nanosheets (cyan line) exhibits an intermediate decrease of 20% in 75 h. Cross-section high-angle annular dark-field (HAADF) scanning TEM images of the 7 $mg_{Pt}\ cm^{-2}$ MEAs after the 75 h runs (Fig. 6b–d) confirm that all three Pt nanomaterials are structurally modified during MEA operation (compare Fig. 5a with 6c, Fig. 5b with 6b, and Fig. 5d with 6d). The images also confirm the formation of holes in the nanosheets; close examination of the images shows that the flat nanosheets and nanospheres retain their overall structures (Fig. 6b, c) but the spaces between the arms of the dendritic sheets are partially filled in leaving many 2–5 nm pores that are visible as dark spots in Fig. 6b, c. This is in contrast with the particles of Pt black, which fuse and grow in size giving particles ranging from 10 to 30 nm in diameter (Fig. 6d). The Pt nanospheres

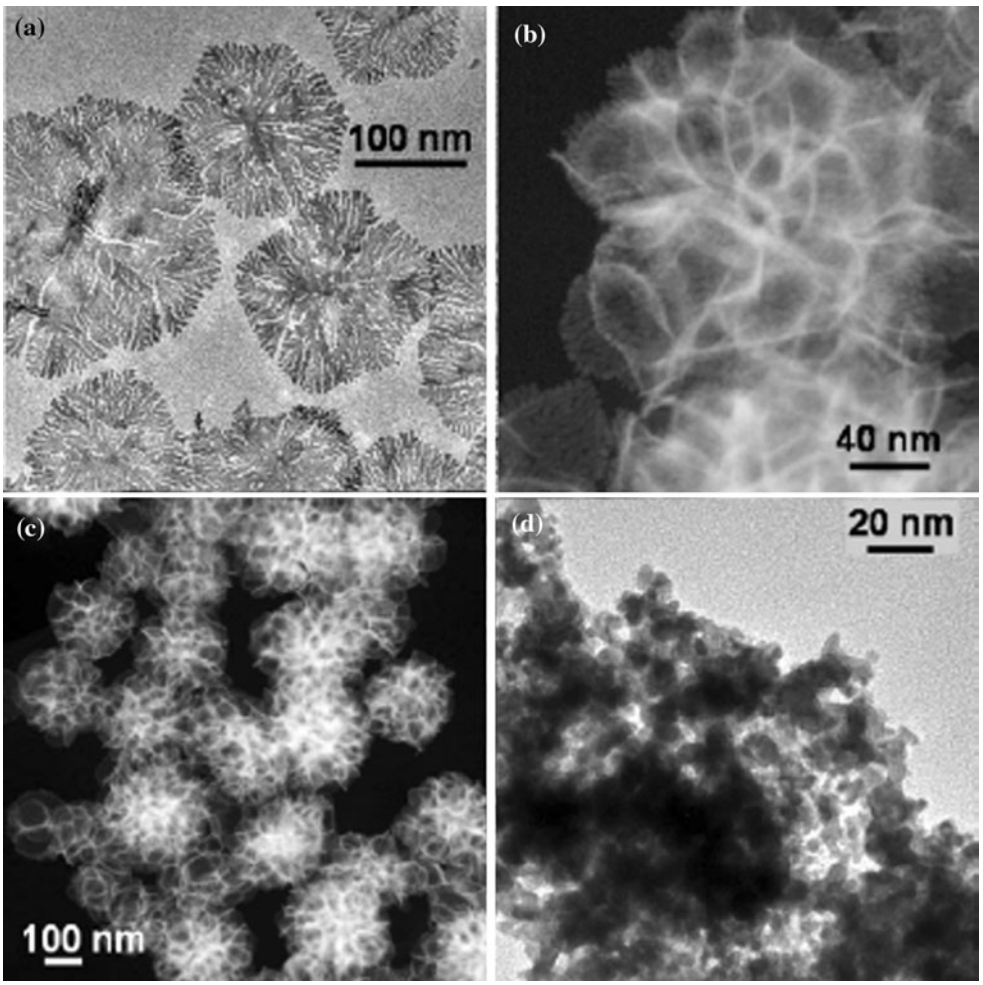

Fig. 5 **a** Bright-field TEM image of flat dendritic platinum nanosheets, **b**, **c** HAADF scanning TEM dark-field images of foamlike Pt nanospheres composed of convoluted dendritic platinum nanosheets, and **d** bright-field TEM image of HiSPEC 1,000 Pt black. Reproduced from [67], copyright 2009, with permission from the American Chemical Society

likely showed less structural changes than the flat nanosheets because the convoluted sheets inside the spheres are protected from the rapid ripening that would result from nanosheet stacking. Both the dendritic nanostructures are superior to unsupported Pt black, where the structural changes are dominated by rapid interfacial ripening resulting in the greatest loss of surface area. Pd–Pt bimetallic nanodendrites consisting of a dense array of Pt branches on a Pd core were synthesized by reducing K_2PtCl_4 with L-ascorbic acid in the presence of uniform Pd nanocrystal seeds [68, 69]. The Pt branches supported on faceted Pd nanocrystals exhibited relatively large surface areas and certain active facets (particularly the {111} facet). MA for the ORR of Pd–Pt nanodendrites was 2.5 times higher than that of Pt/C and five times higher than that of Pt black [68]. The Pd–Pt nanodendrites were also more active for formic acid oxidation than foam-like Pt nanostructures prepared in the absence of Pd seeds under otherwise identical conditions [69]. Lin et al. [70], employing different temperatures and concentrations of sodium dodecyl sulfate, obtained Pt nanosponges, Pt nanonetworks, and Pt nanodendrites from the reduction of H_2PtCl_6 via galvanic replacement reactions with Te nanowires. The ratio of the forward anodic peak current density (I_f) to the backward anodic peak current density (I_b) can be used to describe the suitability of a catalyst for methanol oxidation. A low I_f/I_b ratio indicates poor electro-oxidation of methanol to carbon dioxide during the forward scan, and excessive accumulation of carbonaceous intermediates on the catalyst surface. A high I_f/I_b ratio shows the converse case. Pt nanodendrite-, Pt nanosponge-, and Pt nanonetwork-coated electrodes featured I_f/I_b ratios of 2.88, 2.66, and 2.18, respectively. Thus, the MOR activity follows the order Pt nanodendrites > Pt nanosponges > Pt nanonetworks. The I_f/I_b ratios of Pt nanosponge- and nanodendrite-coated electrodes decreased by less than 10% after 500 scans, whereas that of Pt nanonetwork-coated electrode decreased by 20%.

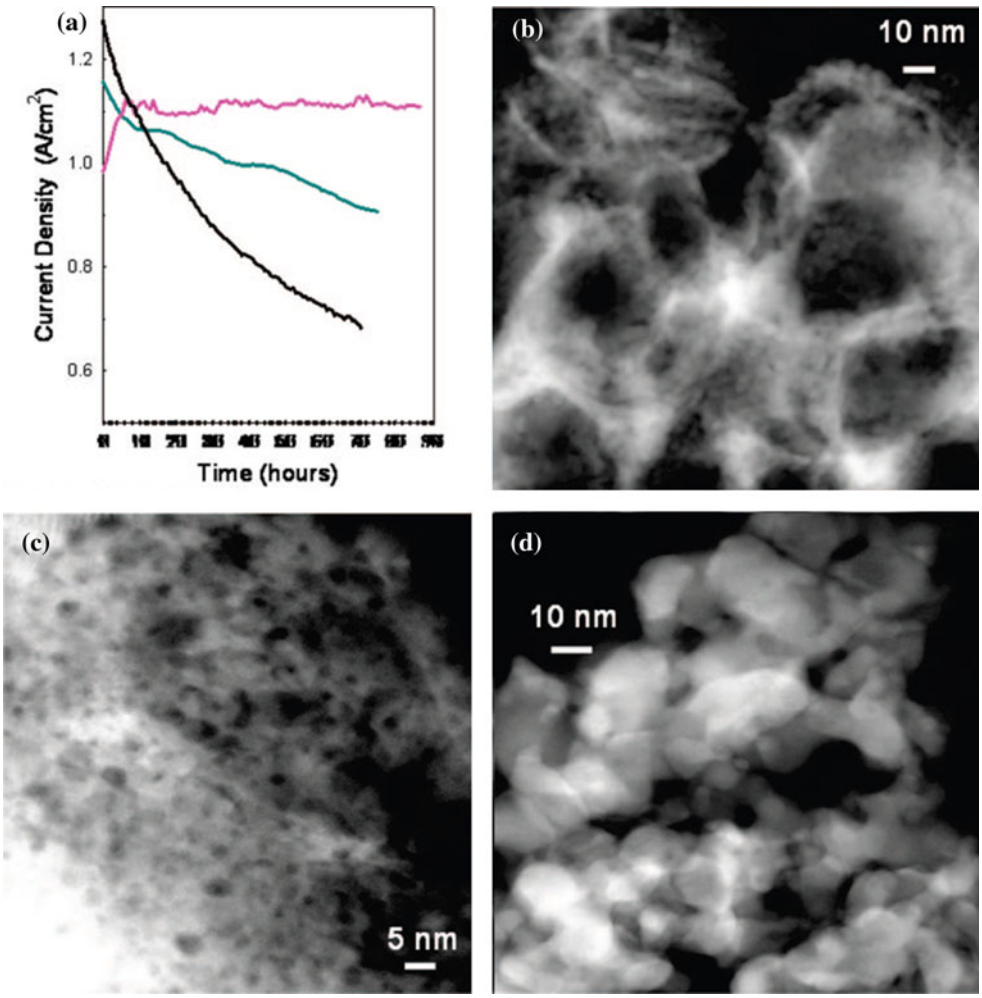

Fig. 6 **a** Durability tests of MEAs at 0.5 V for the 7 mg_{Pt} cm^{-2} loadings of dendritic Pt nanospheres (*magenta*), nanosheets (*cyan*), and platinum-black (*black*). Dark-field TEM images of sections of the MEA made with the Pt nanospheres (**b**), flat nanosheets (**c**), and Pt black (**d**) after nominal 75 h runs. Both the nanospheres and the flat nanosheets show dark circular nanoscale pores in the dendritic sheets. Reproduced from [67], copyright 2009, with permission from the American Chemical Society

Among various nano-architectures, recently nanoflowers (NFs) have emerged as compelling materials because such structured nanomaterials possess porous nature, providing high surface areas and also active centers for electrocatalysis. Teng et al. [71] prepared flowerlike porous platinum nanostructured catalysts by means of a self-organization process at low temperature. The amount of platinum precursor was one of the key factors in the synthesis of platinum nanoflowers (PtNFs). As both kinetic and thermodynamic processes were likely involved in this reaction, the concentration of the precursor could affect the growth of Pt nanoparticles during and after the formation of interconnected nanostructures. The average diameter of the PtNFs was 36 nm. The MOR activity of the nanostructured catalysts was ca. 60 % greater than that of a commercial Pt/C.

Sun et al. [72] synthesized three-dimensional (3D) PtNFs via a simple chemical reduction of H_2PtCl_6 with formic acid at room temperature, using neither template nor surfactant. The PtNFs were composed of metallic Pt nanowires. Numerous nanowires, with lengths of 100–200 nm, were assembled into 3D flower-like superstructures. They investigated the effect of reaction temperature on the morphology of the nanostructures. When the synthesis was performed at 80 °C, the reduction was much faster than at room temperature, and only individual nanoparticles were formed. These observations indicate that a more rapid reduction at higher temperature favors the formation of nanoparticles, suppressing the growth of nanowires. The Pt nanowires were deposited onto carbon paper, which can be used in fuel cells as the charge-collecting electrode. On deposition, they form 3D nanoflowers through a self-organization process, without any functionalization of the carbon paper support. PtNFs adhered to carbon paper, exhibiting an enlarged ECSA, comparable to that of a commercial Pt/C electrode (~ 65 m^2 g^{-1}). Tiwari et al. [73] synthesiszed 3D PtNFs by a potentiostatic pulse plating method on a silicon substrate. Electrochemical study showed that the nanostructured Pt catalyst has a higher activity toward methanol and CO oxidation due to preferential {100} and {110} surface orientations and high surface area of the PtNFs as compared with the Pt thin film

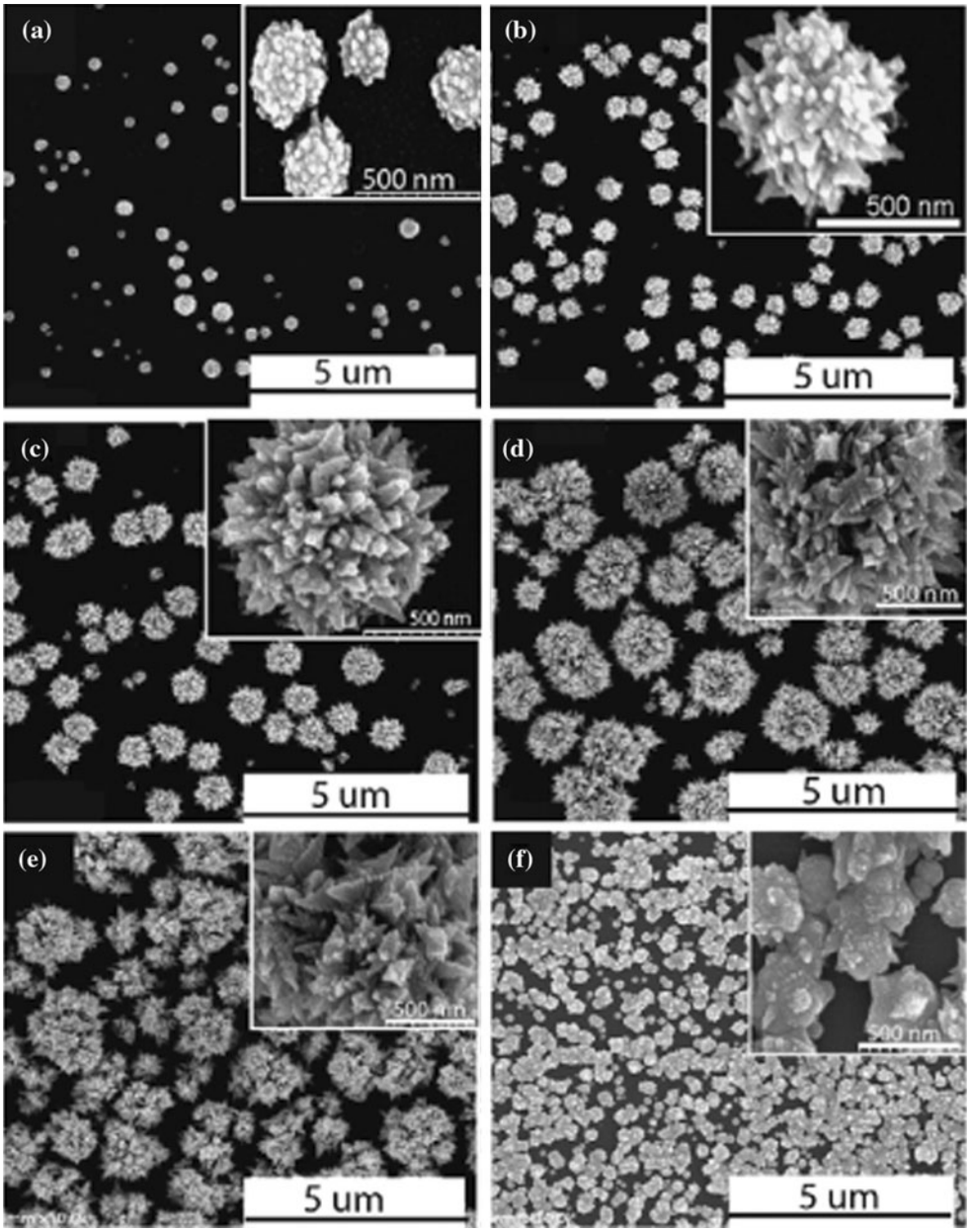

Fig. 7 SEM images of Pt nanostructures electrodeposited on ITO at −0.2 V under various conditions: 1 in 3.0 mM H_2PtCl_6 + 0.5 M H_2SO_4 electrolyte for 25 s (**a**), 400 s (**b**), 1,000 s (**c**), 4,000 s (**d**), and 10,000 s (**e**), and 2 in 3.0 mM H_2PtCl_6 + 0.1 M KCl electrolyte for 2,000 s (**f**). *Insets* are at higher magnifications. Reproduced from [74], copyright 2010, with permission from Elsevier

catalyst. Zhang et al. [74] reported a one-step preparation of porous PtNFs on a clean indium tin oxide (ITO) glass substrate using an electrochemical deposition method. The dynamic growing processes of the PtNFs were characterized by time-coursed SEM measurements (Fig. 7a–e). It was found that the quasi-spherical studded particles were initially formed at the earlier stages (Fig. 7a), which acted as the nuclei for subsequently producing PtNFs. When the deposition time reached to 400 s, many pricks started to form and extruded from the surfaces of the studded spherical particles (Fig. 7b). Further prolonging the growth time to 1,000 s, the perfect PtNFs were formed on the surface of ITO (Fig. 7c). After 1,000 s (Fig. 7d, e), the petals of PtNFs changed gradually, becoming larger with the deposition time. The MOR activity and stability of the PtNFs was much higher than that of Pt nanoparticles. The superior catalytic properties of PtNFs were mainly attributed to their different favorably exposed facets and their increased electrochemical active surface area. A 3D Pd flowerlike nanostructure was synthesized by a modified

polyol process without using a template [75]. A very fast autocatalytic reduction of Pd ions in the second step of the reaction played an important role in the formation of the nanostructure. By the directing effect of oleylamine, three-dimensional Pd nanoflowers were obtained. The porous Pd nanoflowers were more active and more stable than Pd nanoparticles for methanol electro-oxidation in alkaline medium.

Porous structures

Mesoporous Pt and PtRu catalysts

There has been considerable research into the production of ordered mesoporous materials (MPm) (i.e. materials with pores in the 2–50 nm range) through directed templating techniques [76]. Initial work concentrated on the production of metal oxides with well-defined pore sizes. This approach has been significantly broadened by the introduction of liquid crystal-templating materials [77]. Porous platinum films have been produced through either chemical or electrochemical reduction of a system composed of a lyotropic liquid crystal and H_2PtCl_6 [78, 79]. Such porous platinum films have roughness factors of over 200, and are composed of film or particles which typically contain a regular array of cylindrical pores of 1–10 nm in diameter separated by walls of the same thickness [80], as illustrated in Fig. 8a. A TEM image of a Pt mesoporous material is shown in Fig. 8b. In general, significantly increased surface areas were observed compared to employing a plating bath without structure-directing agents. For example, an active surface area increase of 65% for Pt was achieved by liquid crystal-templating compared to depositing in an aqueous electrolyte without a surfactant. The combination of high surface areas, uniform pore diameters, and large particles makes the metallic system of considerable interest for applications in fuel cells. Jiang and Kucernak prepared mesoporous Pt and PtRu alloy from both chemical and electrochemical reduction of H_2PtCl_6 and $RuCl_3$ (only for PtRu) in a normal topology hexagonal mesophase [45, 81–83]. The nanostructured Pt was characterized by a high ECSA of 34.7 $m^2\ g^{-1}$, higher than that of platinized platinum. Electrodeposited PtRu from the liquid crystalline phases consisted of aggregated microspheres with a narrow particle size distribution ranging over 0.5–1.0 μm. It is important to note that these particles are not solid, but have a mesoporous morphology, i.e., each sphere is porous like a sponge [45]. The specific electrochemical surface area of mesoporous PtRu microspheres measured using both the CO adsorption and underpotential deposited Cu stripping techniques is 78–81 $m^2\ g^{-1}$, much larger than that of unsupported precious metal catalysts produced using standard techniques [45]. Both the average diameter of the pores and the thickness of their walls separating them were 2.4 nm. On the basis of the pore size and wall thickness, a mesoporous PtRu film with perfect hexagonal nanostructure would be expected to contain 77.4 vol% PtRu and 22.6 vol% pores. These materials provided high activity toward HCOOH and CH_3OH oxidation reaction and tolerance to CO poisoning [81–83]. The mass and specific surface area activities toward methanol oxidation for the mesoporous PtRu material were higher than those of ultrafine conventional PtRu electrocatalysts. During methanol oxidation there was insignificant formation of CO poisons on these mesoporous Pt and PtRu catalysts, ascribed to the morphology of the material. Successively, they reported the synthesis of PtRu electrocatalyst with ordered porous structure by a solid template route using mesoporous SBA-12 silica [84]. The resultant PtRu material demonstrated regular pore-wall nanostructure, with both the average wall thickness and average diameter of the pores around 3.0 nm, and high activity toward methanol electro-oxidation. Park et al. [85] and Planes et al. [86] evaluated electrodeposited mesoporous Pt (MPPt) electrodes by the liquid crystal-templating method as catalysts for CO and methanol electro-oxidation. Electrochemical analysis revealed a mass activity for MOR higher than that of nonporous Pt [85] or similar to Pt/C [86]. The high current densities, however, are related to low CO_2 conversion efficiencies, as was established by using differential

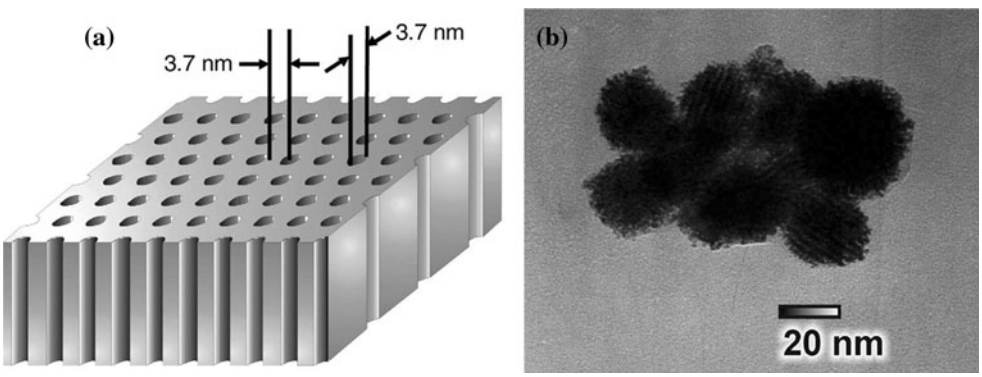

Fig. 8 **a** Schematic diagram of the geometry of the mesoporous platinum catalyst; **b** TEM image of one particle of the mesoporous platinum catalyst. Reproduced from [80], copyright 2003, with permission from Elsevier

electrochemical mass spectrometry in a thin layer flow cell configuration (TLFC-DEMS) [86]. These results were explained considering the especially accessible porous structure of the MPPt, where the possibility of readsorption of partially oxidized products is low.

By the liquid crystal-assisted potentiostatic deposition of platinum, Bauer et al. [87] obtained particles with diameters of about 50 nm and a mesoporous fine structure, reproducing the bulk templating pattern formed by the hexagonal micellar phase. The ORR activity was improved at potentials more negative than 0.95 V versus RHE for the templated catalyst compared to Pt prepared without structure-forming additives. This improvement was partially due to the ~2.7 times larger active Pt surface area and was also a result of the improved intrinsic activity, as indicated by the exchange current density and the surface specific activity.

Nanoporous Pt, Pt-based, and Pd catalysts

Nanoporous materials (NPm) are a subset of porous materials, typically with porosity (volume ratio of pore space to the total volume of the material) greater than 0.4, and pore diameters between 1 and 100 nm. There is not a clear distinction between mesoporous and nanoporous materials. In general, nanoporous materials present a more wide and disordered pore distribution than mesoporous materials. This difference is related to their preparation method: while mesoporous metals are formed by using through directed templating techniques, resulting in an ordered porous structure, nanoporous catalysts are generally prepared by either electrochemical dealloying, such as from $Cu_{0.75}Pt_{0.25}$ [88] and ZnPt [89] alloys, or hydrothermally assisted seed growth [90].

Electrochemical dealloying was used to prepare nanoporous platinum (NPPt) [91] and palladium (NPPd) [92–94] structures. Liu et al. [91] obtained NPPt films with a very high surface area by a selective anodic dissolution of Cu from a PtCu alloy. The surface area of the dealloyed NPPt film was highly enhanced by up to 500 times compared with that of a polycrystalline platinum electrode. This NPPt film exhibited remarkable ORR and MOR activities, with promising applications in fuel cells. Yu et al. [92] synthesized NPPd by electrochemically dealloying multicomponent $Pd_{30}Ni_{50}P_{20}$ metallic glass ribbons. Figure 9a shows a bright-field TEM image of the fully dealloyed sample. The size of the large pores is about 30–60 nm, and the ligaments among those big pores contain a large number of small pores with a size of about 5 nm. The atomic structure of the nanoporous Pd was revealed by HRTEM. The ligaments are found to be comprised of nanocrystals with a grain size of about 5 nm (Fig. 9b). Both the selected-area electron diffraction pattern (inset of Fig. 9b) and energy dispersive X-ray (EDX) spectrum (Fig. 9c) prove that the nanocrystalline phase is fcc Pd with a small amount of residual Ni. The fully dealloyed sample showed high activity for formic acid electro-oxidation, with a broad anodic peak centered at ~0.36 V (vs. RHE), much lower than those from single-crystalline palladium electrodes and a commercial Pd/C catalyst. Wang et al. [93, 94] synthesized NPPd with ultrafine ligament size by dealloying of an Al–Pd alloy in an alkaline solution. Electrochemical measurements indicated that NPPd has significantly high ECSA (23 $m^2\ g^{-1}$),

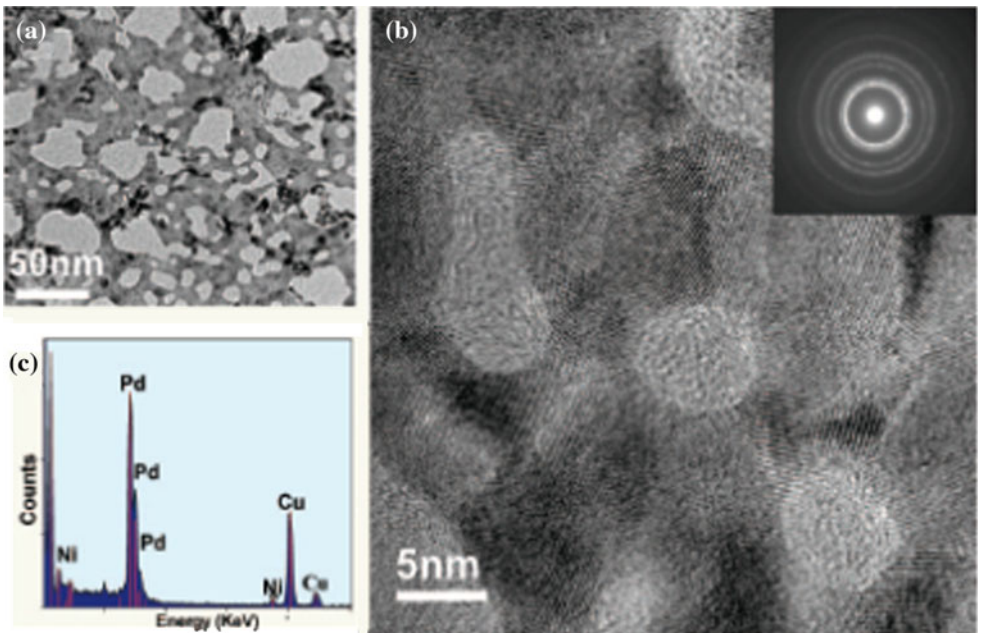

Fig. 9 **a** Bright-field TEM and **b** HRTEM micrograph of hierarchical nanoporous Pd. The *inset* is a selected-area electron diffraction pattern. **c** EDX spectrum of nanoporous Pd. Reproduced from [92], copyright 2008, with permission from the American Chemical Society

and high catalytic activity for electro-oxidation of methanol, ethanol, and formic acid. Peng et al. [90] prepared three-dimensional NPPt network electrodes by a hydrothermal-assisted seed growth process. Electrochemical studies showed that the actual surface area of the NPPt network electrode is over 20 times larger than that of a polycrystalline Pt electrode and that the NPPt network electrode has a much higher MOR activity. The same research group reported on the direct growth of nanoporous Pt and Pt-M networks (where M = Ru, Ir, Pb or Pd) on Ti substrates using the novel one-step hydrothermal method [95]. The active surface areas of the nanoporous Pt-containing electrodes were much larger than that of the polycrystalline Pt electrode. All the nanoporous electrodes showed higher electrocatalytic performance toward methanol and formic acid oxidation than that of the polycrystalline Pt electrode.

Xu and Lin [96] prepared a nanoporous $Pt_{0.9}Pd_{0.1}$ alloy film with high surface area by multi-cycle CV electrodeposition on a glassy carbon surface at room temperature. The method is simple, cost-effective, and adaptable. This homogeneous nanostructured $Pt_{0.9}Pd_{0.1}$ alloy film exhibited high ORR and MOR activity. Nanoporous Pt–Co alloy nanowires with different morphologies and controllable compositions were obtained by dealloying electrodeposited Pt_1Co_{99} nanowires in the presence of porous alumina templates in a mild acidic medium [97]. These nanoporous Pt–Co alloy nanowires showed an enhanced electrocatalytic activity toward methanol oxidation in comparison to state-of-the art Pt/C catalysts. The ECSA of nanoporous Pt–Co nanowires increased with dealloying time, going from 19.4 $m^2\ g^{-1}$ for 10 min dealloying to 46.4 $m^2\ g^{-1}$ for 15 h dealloying.

Metal nanostructures with high specific activity

The shape of Pt nanocrystals plays an important role in determining the performance of an electrocatalyst. In general, the intrinsic reactivity and selectivity of Pt catalysts are controlled by the crystalline structures and morphologies of the particles. Different facets on Pt nanoparticles have different catalytic activities toward fuel cell reactions, due to the distinct adsorption properties of the different chemical species on these facets. In oxygen reduction measurements, the most commonly used electrolytes are $HClO_4$ and H_2SO_4. In the non-adsorbing $HClO_4$, the ORR activity decreased in the order of $\{110\} > \{111\} > \{100\}$ due to the decreased interaction strength between O_2 and different surface structures and increased adsorption of the OH species on these surfaces [98, 99]. For the adsorbing H_2SO_4, instead, the ORR activity decreased in the order of $\{110\} > \{100\} > \{111\}$, by the adsorption and inhibiting effect of bi-sulfate anion on the {111} facets [100].

The oxidation reactions of fuels commonly used in low-temperature fuel cells, such as methanol, formic acid, ethanol, and dimethyl ether, on platinum surfaces are structure sensitive reactions. For methanol oxidation, it has been reported that the Pt {100} facet is more active than the Pt {111} facet [101, 102]. Similarly, formic acid oxidation on the three basal planes of Pt has also been studied and the results demonstrate that the {100} surface is more active than {111} [103]. Tong et al. [104] examined the electro-oxidation of dimethyl ether on Pt{*hkl*} and demonstrate that it is an extremely structure sensitive reaction which takes place almost exclusively on surface sites with {100} symmetry.

Besides the different effect of the three basal low-index planes, oxygen reduction and formic acid, methanol and ethanol electro-oxidation are also influenced by stepped surfaces [105–108]. Stepped surfaces, irrespective of their step site symmetry, showed higher catalytic activity on oxygen reduction than those on basal low-index surfaces [105, 106]. These kind of studies are relevant not only from a fundamental point of view but also from a practical one, because in practical applications the stepped surfaces may be considered as models for surface defects always present on dispersed electrodes. However, little is known about the surface atomic structure of nanoparticles with sizes of practical relevance, which limits the application of fundamental understanding in the reaction mechanisms established on single-crystal surfaces to the development of active, nanoscale catalysts. Recently, Lee et al. [109, 110] characterize and quantify the role of surface steps on Pt nanoparticles in CO and methanol oxidation and in oxygen reduction with sizes of practical relevance. They show that increasing surface steps on Pt nanoparticles of ~ 2 nm lead to enhance the activity of electrochemical oxidation of CO and methanol electro-oxidation [109]. Conversely, they found that the ORR activity is not influenced by surface steps [110]. Furthermore, some nanostructures enclosed within high-index facets could contain more unsaturated atomic steps, edges, and kinks, which are believed to be more catalytically active than the commonly formed nanostructures within low-index facets [13, 111]. On these bases, Pt and Pt-based nanoparticles with certain facets were used for the oxygen electro-reduction and for some electrocatalytic oxidation reactions such as methanol, formic acid and ethanol.

Pt and Pt-based nanocubes

Nanocubes (NCs) are cubic shape nanostructures with 6 facets, 8 corners, and 12 edges. The cubic structure has {100} surface plane and fcc crystal structure. Synthesis of

platinum nanocubes (PtNCs) involves the reduction of a Pt salt using sodium borohydride, alcohol, or hydrogen in the presence of a surfactant, preferably anionic or cationic type [15]. However, the resultant structures are often non-uniformly faceted. As a result, a different strategy based on the polyol method has been reported for the formation of regular nanocubes. In this route PVP is used as the capping agent, in addition to foreign metal species such as Ag and Fe ions for controlling the shape and surface structure [40]. Pt and Pt-based nanocubes showed higher activity for oxygen reduction and methanol, ethanol and dimethyl ether oxidation than homologous polycrystalline spherical nanoparticles [112–120]. Wang et al. [112] synthesized monodisperse 8 nm PtNCs by dissolving $Pt(acac)_2$, oleic acid, and oleylamine in 1-octadecene and heating the solution in the presence of $Fe(CO)_5$. Figure 10a shows the TEM image of the as synthesized 8 nm nanocubes. They are nearly 100% in cubic (or cube like) shape. HRTEM image of a single PtNC (Fig. 10b) shows the Pt lattice fringes with the interfringe distance measured to be 0.19 nm, close to the lattice spacing of the {100} planes at 0.196 nm in the fcc Pt crystal. Figure 10c shows the XRD pattern of the 8 nm PtNCs. Slow evaporation of the hexane dispersion of the 8 nm Pt nanocubes on a silicon substrate led to a textured assembly, as shown in Fig. 10d. The

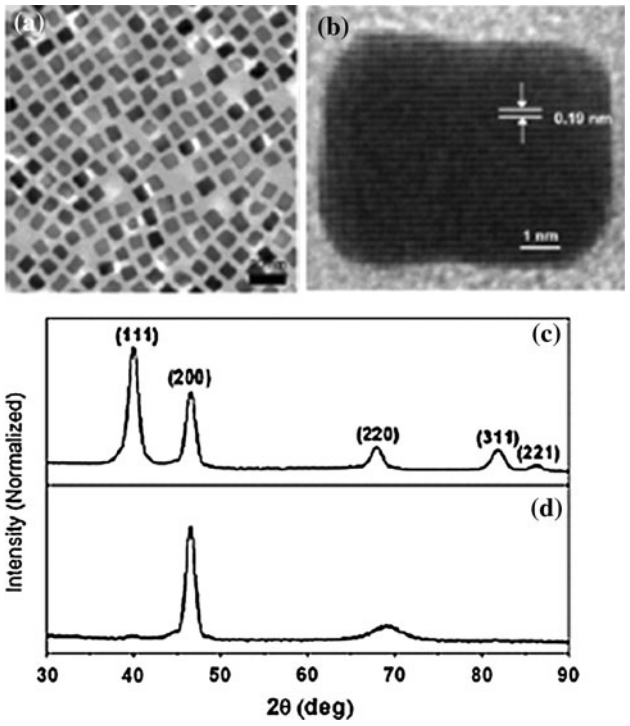

Fig. 10 **a** TEM image of the 8 nm Pt nanocubes; **b** HRTEM image of a single Pt nanocube; **c** XRD pattern of the 8 nm Pt nanocube array; and **d** XRD pattern of the self-assembled 8 nm Pt nanocubes showing (100) texture. Reproduced from Ref. 112, copyright 2007, with permission from the American Chemical Society

strong {200} peak in the diffraction pattern indicates that the Pt nanocubes align flat on the substrate. This further proves that the nanocubes have a very narrow shape distribution. The nanocubes on a carbon paper showed an enhanced specific activity toward ORR in H_2SO_4, over two times as high as that from the commercial spherical 3 nm Pt nanoparticles. Using the method previously described, the same researchers synthesized monodisperse Pt nanoparticles with controlled sizes (3–7 nm) and shapes (polyhedron, truncated cube, and cube) [113]. The ORR activity in H_2SO_4 of 7 nm platinum nanocubes was four times than that of 3 nm polyhedral (or 5 nm truncated cubic) Pt nanoparticles, indicating a dominant effect of the shape. This result was ascribed to the high exposure of the Pt{100} facets, as in H_2SO_4 the ORR activity on the {100} facets is considerably higher than that on the {111} facets [99, 100]. Han et al. [114] prepared PtNCs with particle size of about 3.6 nm by means of PVP and Fe^{3+} ion controllers in polyol process. The PtNCs with dominant {100} faces showed lower onset potential and higher current density for methanol and ethanol electrooxidation than polycrystalline Pt. They considered that the edge of stepped {100} faces in the Pt nanocube catalyst leads to an easier breakage of C–C of CH_3CH_2OH compared to polycrystalline Pt. Xu et al. [115] and Yang et al. [116] compared methanol oxidation on cubic and spherical Pt–Cu nanoparticles. They found that the catalytic activity strongly depends on the particle surface structure. For methanol oxidation, cubic nanostructured Pt–Cu catalysts presented a higher activity than spherical Pt–Cu nanoparticles, implying that the {100}-terminated Pt–Cu nanocubes offer a higher activity toward methanol oxidation than those with mixed crystallographic facets. For formic acid oxidation, instead, spherical Pt–Cu nanoparticles were the most active catalysts at low potentials, whereas cubic nanostructured Pt–Cu catalysts showed the highest activity at high potentials [115]. Lu et al. [117] synthesized PtNCs with preferential {100} surfaces by a colloidal method. The catalytic activity of Pt nanocubes for dimethyl ether electro-oxidation was nearly three times higher than that on commercial available Pt black catalyst. Potential step experiment confirmed that the direct oxidation of dimethyl ether occurs exclusively on long-range ordered {100} terrace sites. After potential step to 1.2 V, the PtNC surfaces were reconstructed and the activity for dimethyl ether electro-oxidation decreased. Nogami et al. [118] synthesized single-crystalline platinum nanocubes with porous morphology by using PVP as the capping agent, and ethylene glycol and HCl as the reducing agents of H_2PtCl_6 and investigated their MOR activity. By controlling the material concentrations and reaction conditions, Pt single crystals of about 5 nm in size with {100} facets, stacked one on top of the other, forming porous nanocubes of

20–80 nm in length, were obtained. For comparison with the porous single-crystalline particles, nonporous and polycrystalline Pt particles were prepared, by reducing H_2PtCl_6 using $AgNO_3$ instead of HCl, forming spherical Pt particles with a diameter of ~8 nm. The mass current density for the MOR of the porous single-crystalline Pt nanoparticles was about three times larger than the current density for the nonporous Pt nanoparticles. The activity enhancement of the porous single-crystalline Pt nanocubes could arise from the assembly of all {100} facets of single crystals in addition to the large surface area of the porous particles. Kang et al. [119] and Choi et al. [120] synthesized Mn–Pt and Pt_9Co nanocubes from platinum acetylacetonate and manganese or cobalt carbonyl in the presence of oleic acid and oleylamine, respectively. The electrocatalytic activity for oxygen reduction and formic acid and methanol oxidation of the Mn–Pt nanocubes and spheres were compared. The catalytic activity of Mn–Pt was shape-dependent. The Mn–Pt nanocubes were more active for formic acid and methanol oxidation than spherical Mn–Pt, and were particularly promising for methanol oxidation. Mn–Pt nanocubes showed higher ORR activity than spherical Mn–Pt in H_2SO_4, while the spherical nanoparticles were more active in $HClO_4$. This implies that, as in the case of Pt [99, 100], the ORR activity of Mn–Pt is higher on {111} than on {100} in $HClO_4$, but higher on {100} than on {111} in H_2SO_4 because of sulfate anion adsorption. Analogously, Choi et al. [120] found that the catalytic activity of Pt_9Co nanocubes in H_2SO_4 is significantly higher than that of spherical Pt_9Co.

Pt nanomultioctahedrons

Lim et al. [42] synthesized highly faceted Pt nanocrystals with a large number of interconnected arms in a quasi-octahedral shape simply by reducing Pt precursor with PVP in the presence of $FeCl_3$. Electron microscopy studies revealed that the MOHPt nanocrystals have a large number of edge, corner, and surface step atoms. TEM image in Fig. 11a shows that the Pt MOH mainly contained Pt nanocrystals in a multiarmed morphology. The average particle size was 20 nm, and the number of arms on each nanocrystal ranged from a few to over 10. The inset of Fig. 11a shows the TEM image of a single Pt nanocrystal with six arms. The

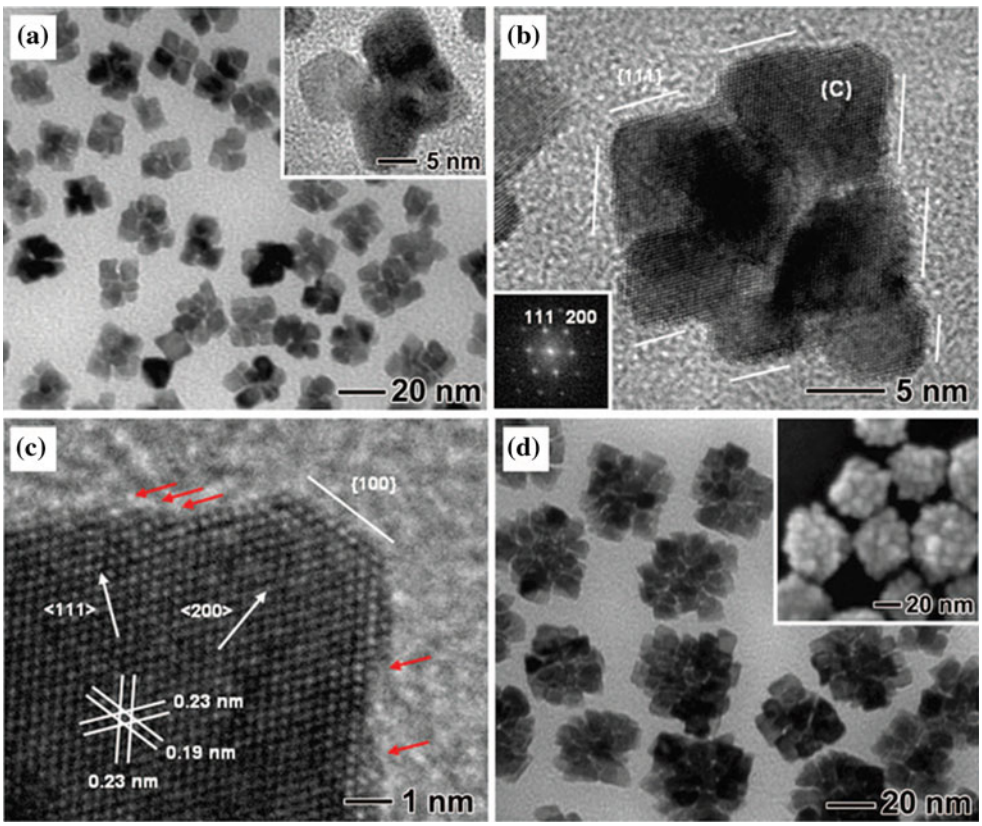

Fig. 11 **a** TEM and (**b**, **c**) (HR-TEM) images of multioctahedral Pt nanocrystals synthesized by heating an aqueous solution containing 7.4 mM H_2PtCl_6, 37 mM PVP, and 36.4 μM $FeCl_3$ at 100 °C for 24 h. In **c**, the atomic steps on the Pt {111} surfaces are indicated by red arrows. **d** TEM and SEM (*inset*) images of Pt nanocrystals prepared under the same conditions as in (**a**) except that the concentration of $FeCl_3$ was increased to 91 μM. Reproduced from [42], copyright 2008, with permission from the American Chemical Society

arms take a quasi-octahedral shape and are perpendicular to each other. Figure 11b shows a HRTEM image of a single MOHPt nanocrystal recorded along the [011] zone axis. Most of the exposed facets are {111} although some of the corners are truncated by {100} facets (see Fig. 11c). The fringes with lattice spacings of 0.19 and 0.23 nm can be indexed as {200} and {111} of fcc Pt, respectively. The MOHPt nanocrystals exhibited rough surfaces with a large number of atomic steps as shown in Fig. 11c. When the reaction was conducted in the presence of 91 μM $FeCl_3$ while maintaining the same concentrations for H_2PtCl_6 and PVP, the reaction was further slowed down. Interestingly, TEM and SEM images of the resulting product revealed that the sample contained MOHPt nanocrystals with an increased average size of 40 nm (Fig. 11d). It can be seen that the number of arms in the Pt nanocrystals increased drastically up to 30–40. These MOHPt nanocrystals exhibited improved ORR specific activity and durability than a commercial Pt/C. The specific activity of 20 nm Pt multioctahedrons in $HClO_4$, was 2.7 times higher than that of a commercial Pt/C (20 wt% 3.2 nm Pt particle size) catalyst. The higher specific activity of the 20 nm Pt multioctahedrons could be attributed to the preferential exposure of {111} facets rich of surface steps on their surfaces compared to Pt nanoparticles on Pt/C catalyst which usually take the shape of a cubo-octahedron with mixed {111} and {100} facets. Being high {111} exposure good for oxygen reduction, but not for methanol oxidation, these nanostructures can be used as ORR methanol tolerant catalysts in DMFCs. However, the mass activity of 20 nm MOHPts was nearly the same as that of 3.2 nm Pt/C catalyst, due to smaller ECSA. Durability tests were performed by RPC between 0.6 and 1.1 V in $HClO_4$ solution at room temperature. After 4,000 cycles, the 20 nm MOHPts showed a slight loss of 5.7% in ECSA, while Pt/C showed a more significant loss of 34%. The higher durability of MOHPts was attributed to the unique morphology, that is, a highly branched structure of interconnected octahedral arms.

Pt nanotetraexahedrons

A number of unconventional shapes covered by high-index facets have been observed in minerals of noble metals. There are four typical single-crystal shapes with high-index surfaces: tetrahexahedron covered by {$hk0$}, trapezohedron by {hkk}, trisoctahedron by {hhl}, and hexoctahedron by {hkl} with, $h > k > l$) [121]. For example, the tetrahexahedron (THH) with O_h symmetry is bound by 24 high-index planes of {$hk0$}, which can be considered as a cube with each face capped by a square-based pyramid. In general, these unconventional shapes are hard to produce using an ordinary chemical method as their surface energies are too high. However, Tian et al. [43] obtained platinum THH nanoparticles by an electrochemical treatment of Pt nanospheres supported on glassy carbon by a square-wave potential. The activity per unit surface area for the electro-oxidation of ethanol and formic acid was superior to that of Pt nanospheres and the commercial 3.2 nm Pt/C catalysts. The enhancement varied from 200 to 400%, depending on electrode potential. This enhanced catalytic activity may be attributed to the high density of stepped atoms on the surfaces of THH Pt nanocrystals.

Conclusions

Unsupported platinum-black nanoparticles were the first-generation low-temperature fuel cell catalysts used in a practical system. These catalysts are more durable than carbon-supported platinum, but suffer from low surface area and low utilization, leading to expensive fuel cells. By taking advantage of the recent advances in nanotechnology, a new generation of unsupported catalysts with high SSA, such as metal NTs, NWs, NDs, and NFs, was introduced, having, because of their unique nanostructures, the potential to combine the advantages of unsupported and carbon-supported catalysts while overcoming their drawbacks. In particular, they possess high surface area, high utilization, high activity, and high stability.

An interesting comparison can be made between fuel cell-unsupported catalysts and carbon supports for fuel cell catalysts. In both cases, due to their high surface area and/or stability, nanotube and mesoporous materials have been proposed as substitutes of conventional materials, that is, spherical metal nanoparticles and carbon blacks, respectively. In both cases, directly for the metal nanostructures, and indirectly for the carbon nanostructures, by increasing metal dispersion with the decrease of the size of supported metal particle [122], an increase of the specific surface area, and, as a consequence, of the catalytic activity of the catalysts is attained.

Meso/nanoporous metal structures possess very high surface area, and, as a consequence, high catalytic activity than conventional non-porous catalysts. Their stability, however, has not been tested: due to the high porosity, likely their stability could be low.

Metal nanocrystals with well-defined and controllable shapes to improve their SA have been obtained by a number of chemical routes. Conventional metal polyhedrons, such as cubes, octahedrons, and tetrahedrons, and their overgrown structures, such as multipods, have all been obtained in reasonably high yields, as well as some unconventional shapes, such as tetrahexahedrons. Compared to commercially available catalysts, these well-defined nanocrystals exhibit greatly enhanced activity and selectivity for a range of reactions. The advances in shape-controlled synthesis of Pt nanocrystals provide an opportunity to engineer their

catalytic properties for various electrochemical reactions. Different studies suggested that the shape of a metal nanocrystal affects not only the catalytic reactivity, but also the catalytic selectivity: this feature is important for an eventual use of these nanostructures as oxygen reduction alcohol tolerant catalysts in DAFCs. For example, the exposure of {111} facet is positive for oxygen reduction, but not for methanol oxidation, so nanostructures with high {111} exposure, such as tetrahedrons and octahedrons, can be used as ORR methanol tolerant catalyst in DMFCs. In general, metal nanocrystals enclosed by high-index facets exhibit much higher catalytic activity than those enclosed by low-index facets. A main goal is to tailor the surface structure of the nanocrystals in such a way to increase the electrode activity and durability. It is worth noting that the capping agents used in the production of Pt nanocrystals may alter their characteristics. How the sizes, shapes, surface structures, and capping agents affect the catalytic and electrocatalytic properties of Pt nanocrystals has to be fully understood yet. Then, it will become possible to design a next-generation of electrocatalysts for a suitable use in low-temperature fuel cells. The results of Wang et al. [113] summarize the key issue of this work: the change of particle shape has a higher effect on the catalytic activity of the nanostructured catalysts than the reduction of the size.

The characteristics of these metal nanostructures, the ECSA values and their catalytic activity, and stability in fuel cell conditions are summarized in Table 1. Figure 12a shows the number of papers reporting tests as fuel cell catalysts on metal nanostructures for type of nanostructure: NWs and NCs were the most studied structures, while only one paper was addressed to the activity of MOH and THH structures, respectively. Thus, it is important to confirm the encouraging results reported for these nanocrystals by other works on their shape-electrocatalytic activity relationship. Moreover, unlike the specific activity, the mass activity of Pt MOH and THH is the same or lower than that of conventional Pt/C, owing to their lower ECSA [42, 43]. Therefore, there is still

Table 1 Physical and morphological characteristics, ECSA values, and electrochemical properties of metal nanostructures

Catalyst	Physical and morphological characteristics	ECSA (best values) $m^2\ g^{-1}$	Electrochemical properties	References
Pt and Pt–Cu nanotubes	Polycrystalline materials with high surface area, anisotropic morphology and inner walls, exposure of certain crystal facets	32	Higher MOR, EOR and ORR activity than Pt/C and unsupported spherical Pt. High stability	[46, 52–55]
Pt and Pd nanowires	Extended polycrystalline nanowire network, high surface area	32	Higher MOR and EOR activity of PtNWs and PdNWs than conventional Pt and Pd, respectively. High stability	[48, 49, 56–65]
Dendritic Pt structures	Presence of open dendritic nanostructures and edges and corner atoms, exposure of certain crystal facets. High surface area	18	Higher ORR activity and stability than Pt/C and Pt black	[47, 67–70]
Pt nanoflowers	3D porous flower-like superstructures, high surface area, exposure of certain crystal facets.	65	Higher MOR activity than conventional Pt nanoparticles	[71–75]
Mesoporous Pt and PtRu nanostructures	High surface area, highly porous structure	80	Higher MOR, EOR and ORR activity than conventional unsupported catalysts. Low metal poisoning	[45, 81–87]
Nanoporous Pt, Pd and Pt-based nanostructures	High surface area, highly porous structure	46	Higher MOR, EOR, FAOR and ORR activity than conventional catalysts.	[90–97]
Pt and Pt-based nanocubes	Cubic shape nanostructures with dominant {100} faces	–	Higher MOR, EOR and DME activity than spherical catalysts. Higher ORR activity only in H_2SO_4	[112–120]
Pt multioctahedrons	Branched structure of interconnected octahedral arms. High ratio between exposed {111} and {100} facets and presence of surface steps	–	Higher ORR specific activity and stability than Pt/C	[42]
Pt tetrahexahedrons	High-index {730}, {210}, and/or {520} faces and high density of stepped atoms on surfaces.	–	Higher EOR and FAOR specific activity than Pt/C	[43]
Conventional unsupported Pt 5–6 nm		15.5	Lower mass activity and higher stability than Pt/C	[47]

much room regarding the optimization of the type of materials, and further attempts have to address to improve the synthesis technique so obtain Pt MOH and THH nanocrystals with smaller particle size. As can be seen in Fig. 12b, the number of these papers considerably increased in the last years: the growing interest on these nanostructures as fuel cells catalysts is demonstrated by the fact that ca. 55% of the papers have been published in the years 2009 and 2010. However, as shown in Fig. 12c, only in a very few number of papers these nanostructure have been tested in fuel cells. To confirm the excellent results obtained by electrochemical measurements such as CV and CA, tests in PEMFCs and in DAFC have to be carried out to evaluate their catalytic activity and selectivity in practical applications.

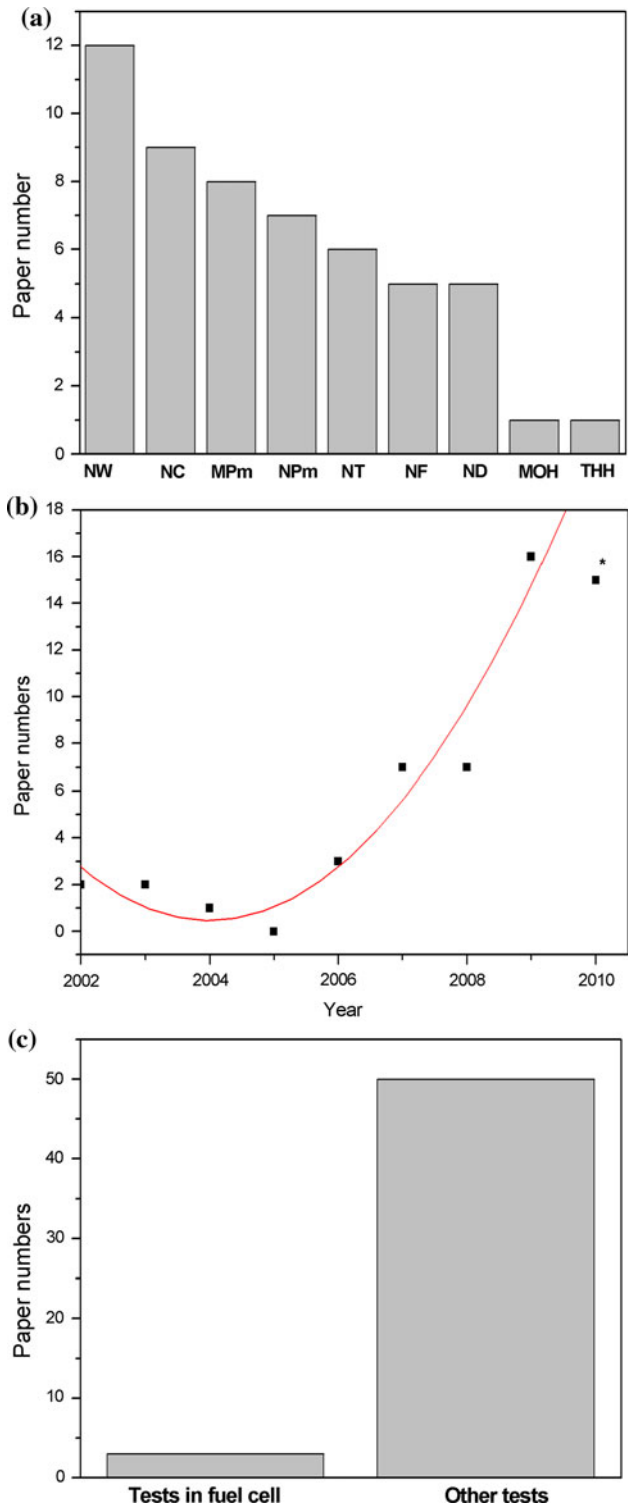

Fig. 12 Number of papers reporting tests as fuel cell catalysts on metal nanostructures for type of nanostructure (**a**), for year (**b**), and for type of test (**c**). * At 31/09/2010

A considerable problem is that the surface structure of the nanostructured catalysts with improved SA can be unstable during PEM fuel cell reactions, especially those with high-index planes and unsaturated atomic steps, edges, and kinks, all of which are active sites for crystal growth. Due to the morphological changes that Pt nanostructured catalysts undergo during fuel cell operation, these facets may easily be deactivated, resulting in degradation of their catalytic activity [111]. Therefore, future research has to be addressed to achievement of means of overcoming the poor thermal and mechanical stability of some of these structures without altering symmetry and stoichiometry.

Moreover, Pt and Pt-based nanocubes have been proposed as catalyst for oxygen reduction on the basis of experiments in H_2SO_4, where the {100} facet is more active than the {111} facet. However, excellent agreement observed between the ORR activities measured in $HClO_4$, where the {111} facet is more active than the {100} facet, and by tests in PEMFCs [25]. Thus, in PEMFCs the use of Pt nanocubes sa catalysts for the ORR is not appropriate, whereas tetrahedral and octahedral Pt nanocrystals, enclosed by {111} facets, are suitable catalysts for oxygen reduction. A recent work of Zhang et al. [123] goes in this direction: they synthesized monodisperse Pt_3Ni nanoctahedrons and nanocubes, enclosed by {111} and {100} facets, respectively, via a high-temperature organic solution chemistry approach. They found that the ORR activity in $HClO_4$ solution on the Pt_3Ni nanoctahedrons is $\sim$5-fold higher than that of nanocubes with a similar size. Future works should be addressed to the synthesis of stable tetrahedral and octahedral Pt nanocrystals with small particle size.

Acknowledgements The authors thank the Conselho Nacional de Desenvolvimento Científico e Tecnológico (CNPq, Proc. 310151/2008-2) and Fundação de Amparo a Pesquisa do Estado de São Paulo (FAPESP) for financial assistance to the project.

References

1. Solid Polymer Electrolyte Fuel Cell Technology Program (1980) In: Test report BU #1 and BU #2 (1.1 ft^2). Direct Energy Conversion Programs, General Electric Co., TRP-76 Contract NAS 9-15286

2. Srinivasan S, Ticianelli EA, Derouin CR, Redondo A (1988) J Power Sources 22:359
3. Costamagna P, Srinivasan S (2001) J Power Sources 102:242
4. Wilson MS, Gottesfeld S (1992) J Electrochem Soc 139:L28
5. Wilson MS, Valerio JA, Gottesfeld S (1995) Electrochim Acta 40:355
6. Liu L, Pu G, Viswanathan R, Fan QB, Liu RX, Smotkin ES (1998) Electrochim Acta 43:3657
7. Kangasniemi KH, Condit DA, Jarvi TD (2004) J Electrochem Soc 151:E125
8. Maass S, Finsterwalder F, Frank G, Hartmann R, Merten C (2008) J Power Sources 176:444
9. Stevens DA, Dahn JR (2005) Carbon 43:179
10. Antolini E, Gonzalez ER (2009) Solid State Ionics 180:746
11. Ren XM, Wilson MS, Gottesfeld S (1996) J Electrochem Soc 143:L12
12. Aricò AS, Shukla AK, El-Khatib KM, Creti P, Antonucci V (1999) J Appl Electrochem 29:671
13. Chen JY, Lim B, Lee EP, Xia YN (2009) Nano Today 4:81
14. Peng ZM, Yang H (2009) Nano Today 4:143
15. Subhramannia M, Pillai VK (2008) J Mater Chem 18:5858
16. Bing YH, Liu HS, Zhang L, Ghosh D, Zhang JJ (2010) Chem Soc Rev 39:2184
17. Kinoshita K (1990) J Electrochem Soc 137:845
18. Peuckert M, Yoneda T, Della Betta RA, Boudart M (1986) J Electrochem Soc 133:944
19. Sattler ML, Ross PN (1986) Ultramicroscopy 20:21
20. Gamez A, Richard D, Gallezot P, Gloaguen F, Faure R, Durand R (1996) Electrochim Acta 41:307
21. Antoine O, Bultel Y, Durand R (2001) J Electroanal Chem 499:85
22. Takasu Y, Ohashi N, Zhang XG, Murakami Y, Minagawa H, Sato S, Yahikozawa K (1996) Electrochim Acta 41:2595
23. Mukerjee S, McBreen J (1998) J Electroanal Chem 448:163
24. Mayrhofer KJJ, Blizanac BB, Arenz M, Stamenkovic VR, Ross PN, Markovic NM (2005) J Phys Chem B 109:14433
25. Gasteiger HA, Kocha SS, Sompalli B, Wagner FT (2005) Appl Catal B 56:9
26. Kabbabi A, Gloaguen F, Andolfatto F, Durand R (1994) J Electroanal Chem 373:251
27. Frelink T, Visscher W, Van Veen JAR (1995) J Electroanal Chem 382:65
28. Zeng JH, Lee JY, Zhou WJ (2006) Appl Catal A 308:99
29. Narayanan R, El-Sayed MA (2004) Nano Lett 4:1343
30. Baletto F, Ferrando R (2005) Rev Mod Phys 77:371
31. Ahmadi TS, Wang ZL, Green TC, Henglein A, El-Sayed MA (1996) Science 272:1924
32. Chu D, Gilman (1996) J Electrochem Soc 143:1685
33. Park K, Choi J, Kwon B, Lee S, Sung Y, Ha H, Hong S, Kim H, Wieckowski A (2002) J Phys Chem B 106:1869
34. Wang Y, Ren J, Deng K, Gui L, Tang Y (2000) Chem Mater 12:1622
35. Bonnemann H (1995) Stud Surf Sci Catal 91:185
36. Zhang X, Tsang K, Chan K (2004) J Electroanal Chem 573:1
37. Sun S, Murray CB, Weller D, Folks L, Moser A (2000) Science 287:1989
38. Ould Ely T, Pan C, Amiens C, Chaudret B, Dassenoy F, Lecante P, Casanove MJ, Mosset A, Respaund M, Broto JM (2000) J Phys Chem B 104:695
39. Lee H, Habas SE, Kweskin S, Butcher D, Somorjai GA, Yang P (2006) Angew Chem Int Ed 45:7824
40. Song H, Kim F, Connor S, Somorjai GA, Yang P (2005) J Phys Chem B 109:188
41. Chen JY, Herricks T, Xia YN (2005) Angew Chem Int Ed 44:2589
42. Lim BW, Lu XM, Jiang MJ, Camargo PHC, Cho EC, Lee EP, Xia YN (2008) Nano Lett 8:4043
43. Tian N, Zhou ZY, Sun SG, Ding Y, Wang ZL (2007) Science 316:732
44. Tiemann M (2008) Chem Mater 20:961
45. Jiang JH, Kucernak A (2004) Chem Mater 16:1362
46. Chen ZW, Waje M, Li WZ, Yan YS (2007) Angew Chem Int Ed 46:4060
47. Song YJ, Steen WA, Pena D, Jiang YB, Medforth CJ, Huo QS, Pincus JL, Qiu Y, Sasaki DY, Miller JE, Shelnutt JA (2006) Chem Mater 18:2335
48. Song Y, Garcia RM, Dorin RM, Wang HR, Qiu Y, Coker EN, Steen WA, Miller JE, Shelnutt JA (2007) Nano Lett 7:3650
49. Wang H, Xu CW, Cheng FL, Jiang SP (2007) Electrochem Commun 9:1212
50. Zhou HJ, Zhou WP, Adzic RR, Wong SS (2009) J Phys Chem C 113:5460
51. Garbarino S, Ponrouch A, Pronovost S, Guay D (2009) Electrochem Commun 11:1449
52. Bi YP, Lu GX (2009) Electrochem Commun 11:45
53. Zhang XY, Dong DH, Li D, Williams T, Wang HT, Webley PA (2009) Electrochem Commun 11:190
54. Zhang XY, Li D, Dong DH, Wang HT, Webley PA (2010) Mater Lett 64:1169
55. Gorzny ML, Walton AS, Evans SD (2010) Adv Funct Mater 20:1295
56. Zhao GY, Xu CL, Guo DJ, Li H, Li HL (2007) Appl Surf Sci 253:3242
57. Song YJ, Han SB, Park KW (2010) Mater Lett 64:1981
58. Ksar F, Surendran G, Ramos L, Keita B, Nadjo L, Prouzet E, Beaunier P, Hagege A, Audonnet F, Remita H (2009) Chem Mater 21:1612
59. Kim JM, Joh H-I, Jo SM, Ahn DJ, Ha HY, Hong S-A, Kim S-K (2010) Electrochim Acta 55:4827
60. Choi SM, Kim JH, Jung JY, Yoon EY, Kim WB (2008) Electrochim Acta 53:5804
61. Garbarino S, Ponrouch A, Pronovost S, Gaudet J, Guay D (2009) Electrochem Commun 11:1924
62. Yuan Q, Zhou ZY, Zhuang J, Wang X (2010) Chem Mater 22:2395
63. Koenigsmann C, Zhou W, Adzic RR, Sutter E, Wong SS (2010) Nano Lett 10:2806
64. Liang ZX, Zhao TS (2007) J Phys Chem C 111:8128
65. Du SF (2010) J Power Sources 195:289
66. Wang L, Wang HJ, Nemoto Y, Yamauchi Y (2010) Chem Mater 22:2835
67. Song YJ, Hickner MA, Challa SR, Dorin RM, Garcia RM, Wang HR, Jiang YB, Li P, Qiu Y, van Swol F, Medforth CJ, Miller JE, Nwoga T, Kawahara K, Li W, Shelnutt JA (2009) Nano Lett 9:1534
68. Lim B, Jiang MJ, Camargo PHC, Cho EC, Tao J, Lu XM, Zhu YM, Xia YA (2009) Science 324:1302
69. Lim B, Jiang MJ, Yu T, Camargo PHC, Xia YN (2010) Nano Res 3:69
70. Lin ZH, Lin MH, Chang HT (2009) Chem Eur J 15:4656
71. Teng XW, Liang XY, Maksimuk S, Yang H (2006) Small 2:249
72. Sun SH, Yang DQ, Villers D, Zhang GX, Sacher E, Dodelet JP (2008) Adv Mater 20:571
73. Tiwari JN, Pan FM, Lin KL (2009) New J Chem 33:1482
74. Zhang H, Zhou W, Du P, Yang P, Wang C (2010) Electrochem Commun 12:882
75. Yin Z, Zheng HJ, Ma D, Bao XH (2009) J Phys Chem C 113:1001
76. Zhao DY, Yang PD, Huo QS, Chmelka BF, Stucky GD (1998) Curr Opin Solid State Mater Sci 3:111

77. Raimondi ME (1999) Liq Cryst 26:305
78. Elliott JM, Birkin PR, Bartlett PN, Attard GS (1999) Langmuir 15:7411
79. Elliott JM, Attard GS, Bartlett PN, Coleman BRB, Merckel DAS, Owen JR (1999) Chem Mater 11:3602
80. Kucernak A, Jiang JH (2003) Chem Eng J 93:81
81. Jiang JH, Kucernak A (2002) J Electroanal Chem 520:64
82. Jiang JH, Kucernak A (2002) J Electroanal Chem 533:153
83. Jiang JH, Kucernak A (2003) J Electroanal Chem 543:187
84. Jiang JH, Kucernak (2009) Electrochem Commun 11:623
85. Park EK, Lee JK, Kim YS, Kim GP, Baeck SH (2008) J Phys Chem Solids 69:1284
86. Planes GA, Garcia G, Pastor E (2007) Electrochem Commun 9:839
87. Bauer A, Wilkinson DP, Gyenge EL, Bizzotto D, Ye S (2009) J Electrochem Soc 156:B1169
88. Pugh DV, Dursun A, Corcoran SG (2003) J Mater Res 18:216
89. Huang JF, Sun IW (2004) Chem Mater 16:1829
90. Peng XS, Koczkur K, Nigro S, Chen AC (2004) Chem Commun 2872-2873
91. Liu HT, He P, Li ZY, Li JH (2006) Nanotechnology 17:2167
92. Yu JS, Ding Y, Xu CX, Inoue A, Sakurai T, Chen MW (2008) Chem Mater 20:4548
93. Wang XG, Wang WM, Qi Z, Zhao CC, Ji H, Zhang ZH (2009) Electrochem Commun 11:1896
94. Wang XG, Wang WM, Qi Z, Zhao CC, Ji H, Zhang ZH (2010) J Alloy Comp 508:463
95. Wang JP, Holt-Hindle P, MacDonald D, Thomas DF, Chen AC (2008) Electrochim Acta 53:6944
96. Xu YH, Lin XQ (2007) J Power Sources 170:13
97. Liu L, Pippel E, Scholz R, Gosele U (2009) Nano Lett 9:4352
98. Markovic NM, Adzic RR, Cahan BD, Yeager EB (1994) J Electroanal Chem 377:249
99. Perez J, Villullas HM, Gonzalez ER (1997) J Electroanal Chem 435:179
100. Markovic NM, Gasteiger HA, Ross PN (1995) J Phys Chem 99:3411
101. Herrero E, Franaszczuk K, Wieckowski A (1994) J Phys Chem 98:5074
102. Housmans THM, Wonders AH, Koper MTM (2006) J Phys Chem B 110:10021
103. Clavilier J (1987) J Electroanal Chem 236:87
104. Tong Y, Lu L, Zhang Y, Gao Y, Yin G, Osawa M, Ye S (2007) J Phys Chem C 111:18836
105. Macia MD, Campina JM, Herrero E, Feliu JM (2004) J Electroanal Chem 564:141
106. Kuzume A, Herrero E, Feliu JM (2007) J Electroanal Chem 599:333
107. Solla-Gullon J, Vidal-Iglesias FJ, Lopez-Cudero A, Garnier E, Feliu JM, Aldaz A (2006) Phys Chem Chem Phys 10:3689
108. Colmati F, Tremiliosi G, Gonzalez ER, Berna A, Herrero E, Feliu JM (2009) Phys Chem Chem Phys 11:9114
109. Lee SW, Chen SO, Sheng WC, Yabuuchi N, Kim YT, Mitani T, Vescovo E, Shao-Horn Y (2009) J Am Chem Soc 131:15669
110. Lee SW, Chen S, Suntivich J, Sasaki K, Adzic RR, Shao-Horn Y (2010) J Phys Chem Lett 1:1316
111. Narayanan R, El-Sayed MA (2005) J Phys Chem B 109:12663
112. Wang C, Daimon H, Lee Y, Kim J, Sun S (2007) J Am Chem Soc 129:6974
113. Wang C, Daimon H, Onodera T, Koda T, Sun SH (2008) Angew Chem Int Ed 47:3588
114. Han SB, Song YJ, Lee JM, Kim JY, Park KW (2008) Electrochem Commun 10:1044
115. Xu D, Liu ZP, Yang HZ, Liu QS, Zhang J, Fang JY, Zou SZ, Sun K (2009) Angew Chem Int Ed 48:4217
116. Yang H, Dai L, Xu J, Fang J, Zou S (2010) Electrochim Acta 55:8000
117. Lu LL, Yin GP, Wang ZB, Gao YZ (2009) Electrochem Commun 11:1596
118. Nogami M, Koike R, Jalem R, Kawamura G, Yang Y, Sasaki Y (2010) J Phys Chem Lett 1:568
119. Kang YJ, Murray CB (2010) J Am Chem Soc 132:7568
120. Choi SI, Choi R, Han SW, Park JT (2010) Chem Commun 46:4950
121. Xiong YJ, Wiley B, Xia YN (2007) Angew Chem Int Ed 46:7157
122. Antolini E (2009) Appl Catal B 88:1
123. Zhang J, Yang HZ, Fang JY, Zou SZ (2010) Nano Lett 10:638